

## Accelerated Article Preview

# Omicron escapes the majority of existing SARS-CoV-2 neutralizing antibodies

---

Received: 7 December 2021

---

Accepted: 23 December 2021

---

Accelerated Article Preview

---

Published online: 23 December 2021

---

Cite this article as: Cao, Y. et al. Omicron escapes the majority of existing SARS-CoV-2 neutralizing antibodies *Nature* <https://doi.org/10.1038/d41586-021-03796-6> (2021).

---

Yunlong Cao, Jing Wang, Fanchong Jian, Tianhe Xiao, Weiliang Song, Ayijiang Yisimayi, Weijin Huang, Qianqian Li, Peng Wang, Ran An, Jing Wang, Yao Wang, Xiao Niu, Sijie Yang, Hui Liang, Haiyan Sun, Tao Li, Yuanling Yu, Qianqian Cui, Shuo Liu, Xiaodong Yang, Shuo Du, Zhiying Zhang, Xiaohua Hao, Fei Shao, Ronghua Jin, Xiangxi Wang, Junyu Xiao, Youchun Wang & Xiaoliang Sunney Xie

---

This is a PDF file of a manuscript that has been peer reviewed and accepted for publication in *Nature* and is provided in this format here as a response to the exceptional public-health crisis. This accepted manuscript will continue through the processes of copy editing and formatting to publication of a finalized version of record on nature.com. Please note there may be errors present in this version, which may affect the content, and all legal disclaimers apply.

# 1 Omicron escapes the majority of existing SARS-CoV-2 neutralizing antibodies

2  
3 Yunlong Cao<sup>1,2,#,\*</sup>, Jing Wang<sup>1,3,#</sup>, Fanchong Jian<sup>1,4,#</sup>, Tianhe Xiao<sup>1,5,#</sup>, Weiliang  
4 Song<sup>1,3,#</sup>, Ayijiang Yisimayi<sup>1,3,#</sup>, Weijin Huang<sup>6,#</sup>, Qianqian Li<sup>6</sup>, Peng Wang<sup>1</sup>, Ran An<sup>1</sup>,  
5 Jing Wang<sup>1</sup>, Yao Wang<sup>1</sup>, Xiao Niu<sup>1,4</sup>, Sijie Yang<sup>1,7</sup>, Hui Liang<sup>1</sup>, Haiyan Sun<sup>1</sup>, Tao Li<sup>6</sup>,  
6 Yuanling Yu<sup>6</sup>, Qianqian Cui<sup>6</sup>, Shuo Liu<sup>6</sup>, Xiaodong Yang<sup>8</sup>, Shuo Du<sup>3</sup>, Zhiying Zhang<sup>3</sup>,  
7 Xiaohua Hao<sup>9</sup>, Fei Shao<sup>1</sup>, Ronghua Jin<sup>9</sup>, Xiangxi Wang<sup>10,\*</sup>, Junyu Xiao<sup>2,3,\*</sup>, Youchun  
8 Wang<sup>6,\*</sup>, Xiaoliang Sunney Xie<sup>1,2,\*</sup>

9  
10 <sup>1</sup>Biomedical Pioneering Innovation Center (BIOPIC), Peking University, Beijing, P.R.  
11 China.

12 <sup>2</sup>Beijing Advanced Innovation Center for Genomics (ICG), Peking University, Beijing,  
13 P.R. China.

14 <sup>3</sup>School of Life Sciences, Peking University, Beijing, P.R. China.

15 <sup>4</sup>College of Chemistry and Molecular Engineering, Peking University, Beijing, P.R.  
16 China.

17 <sup>5</sup>Joint Graduate Program of Peking-Tsinghua-NIBS, Academy for Advanced  
18 Interdisciplinary Studies, Peking University, Beijing, China.

19 <sup>6</sup>Division of HIV/AIDS and Sex-transmitted Virus Vaccines, Institute for Biological  
20 Product Control, National Institutes for Food and Drug Control (NIFDC), Beijing, P.R.  
21 China.

22 <sup>7</sup>Tsinghua-Peking Center for Life Sciences, Beijing, P.R. China.

23 <sup>8</sup>Beijing YouAn Hospital, Capital Medical University, Beijing, P.R. China.

24 <sup>9</sup>Beijing Ditan Hospital, Capital Medical University, Beijing, P.R. China.

25 <sup>10</sup>CAS Key Laboratory of Infection and Immunity, National Laboratory of  
26 Macromolecules, Institute of Biophysics, Chinese Academy of Sciences, Beijing, P.R.  
27 China.

28 \*Correspondence: Yunlong Cao (yunlongcao@pku.edu.cn); Junyu Xiao  
29 (junyuxiao@pku.edu.cn); Xiangxi Wang (xiangxi@ibp.ac.cn); Youchun Wang  
30 (wangyc@nifdc.org.cn); Xiaoliang Sunney Xie (sunneyxie@biopic.pku.edu.cn)

31 #These authors contributed equally.

32  
33  
34 **Abstract**

35 The SARS-CoV-2 B.1.1.529 variant (Omicron) contains 15 mutations on the receptor-  
36 binding domain (RBD). How Omicron would evade RBD neutralizing antibodies  
37 (NAbs) requires immediate investigation. Here, we used high-throughput yeast display  
38 screening<sup>1,2</sup> to determine the RBD escaping mutation profiles for 247 human anti-RBD  
39 NAbs and showed that the NAbs could be unsupervised clustered into six epitope  
40 groups (A-F), which is highly concordant with knowledge-based structural  
41 classifications<sup>3-5</sup>. Strikingly, various single mutations of Omicron could impair NAbs  
42 of different epitope groups. Specifically, NAbs in Group A-D, whose epitope overlap  
43 with ACE2-binding motif, are largely escaped by K417N, G446S, E484A, and Q493R.  
44 Group E (S309 site)<sup>6</sup> and F (CR3022 site)<sup>7</sup> NAbs, which often exhibit broad  
45 sarbecovirus neutralizing activity, are less affected by Omicron, but still, a subset of  
46 NAbs are escaped by G339D, N440K, and S371L. Furthermore, Omicron pseudovirus  
47 neutralization showed that single mutation tolerating NAbs could also be escaped due  
48 to multiple synergetic mutations on their epitopes. In total, over 85% of the tested NAbs  
49 are escaped by Omicron. Regarding NAb drugs, the neutralization potency of LY-  
50 CoV016/LY-CoV555, REGN10933/REGN10987, AZD1061/AZD8895, and BRII-  
51 196 were greatly reduced by Omicron, while VIR-7831 and DXP-604 still function at  
52 reduced efficacy. Together, data suggest Omicron would cause significant humoral  
53 immune evasion, while NAbs targeting the sarbecovirus conserved region remain most  
54 effective. Our results offer instructions for developing NAb drugs and vaccines against  
55 Omicron and future variants.

56

57 **Main**

58

59 The severe acute respiratory syndrome coronavirus 2 (SARS-CoV-2) variant B.1.1.529  
60 was first reported to the World Health Organization (WHO) on 24 November 2021. It  
61 appears to be rapidly spreading, and the WHO classified it as a variant of concern  
62 (VOC) only two days after, designating it as Omicron <sup>8,9</sup>. An unusually large number  
63 of mutations are found in Omicron, including over 30 in the spike protein (Extended  
64 Data Fig. 1a). The receptor-binding domain, responsible for interacting with the  
65 Angiotensin-Converting Enzyme 2 (ACE2) receptor, bears 15 of these mutations,  
66 including G339D, S371L, S373P, S375F, K417N, N440K, G446S, S477N, T478K,  
67 E484A, Q493R, G496S, Q498R, N501Y, and Y505H. Some of these mutations are  
68 very concerning due to their well-understood functional consequences, such as K417N  
69 and N501Y, which contribute to immune escape and higher infectivity <sup>10-13</sup>. Many other  
70 mutations' functional impacts remain to be investigated.

71

72 The S protein is the target of essentially all NABs found in the convalescent sera or  
73 elicited by vaccines. Most of the N-terminal domain (NTD) neutralizing antibodies  
74 target an antigenic “supersite” in NTD, involving the N3 (residues 141 to 156) and N5  
75 (residues 246 to 260) loops <sup>14,15</sup>, and are thus very prone to NTD mutations. Omicron  
76 carries the Δ143-145 mutation, which would alter the N3 loop and most likely result in  
77 immune escape of most anti-NTD NABs (Extended Data Fig. 1b). Compared to NTD  
78 targeting NABs, RBD targeting NABs are particularly abundant and potent, and display  
79 diverse epitopes. Evaluating how Omicron affects the neutralization capability of anti-  
80 RBD NABs of diverse classes and epitopes is urgently needed.

81

82 RBD-directed SARS-CoV-2 NABs can be assigned into different classes or binding  
83 sites based on structural analyses by cryo-EM or high-resolution crystallography <sup>3-5</sup>;  
84 however, structural data only indicates the contacting amino acids, but does not infer  
85 the escaping mutations for a specific antibody. Recent advances in deep antigen  
86 mutation screening using FACS (fluorescence-activated cell sorting)-based yeast  
87 display platform has allowed the quick mapping of all single amino acid mutations in  
88 the RBD that affect the binding of SARS-CoV-2 RBD NABs <sup>1,16</sup>. The method has  
89 proven highly effective in predicting NAB drug efficacy toward mutations <sup>2</sup>. However,  
90 to study how human humoral immunity may react to highly mutated variants like

91 Omicron requires mutation profiling of a large collection of NABs targeting different  
92 regions of RBD, and FACS-based yeast display mutation screening is limited by low  
93 experimental throughput. Here we further developed a MACS (magnetic-activated cell  
94 sorting) -based screening method which increases the throughput near 100-fold and  
95 could obtain comparable data quality like FACS (Fig 1a, Extended Data Fig. 2). Using  
96 this method, we quickly characterized the RBD escaping mutation profile for a total of  
97 247 NABs (Supplementary Data 1). Half of the NABs were part of the antibodies  
98 identified by us using single-cell VDJ sequencing of antigen-specific memory B cells  
99 from SARS-CoV-2 convalescents, SARS-CoV-2 vaccinees, and SARS-CoV-1  
100 convalescents who recently received SARS-CoV-2 vaccines (Supplementary Data 2).  
101 The other half of NABs were identified by groups worldwide<sup>3,5,6,11,17-40</sup> (Supplementary  
102 Table 1).

103

104 The high-throughput screening capability allowed us to classify these NABs into six  
105 Epitope Groups (A-F) using unsupervised clustering without dependence on structural  
106 studies, and the grouping is highly concordant with the knowledge-based structural  
107 classifications<sup>3-5</sup> (Fig. 1b, c). In particular, Group A-D NABs largely correspond to the  
108 RBS A-D NABs described by Yuan et al.<sup>4</sup> and overlap with the class 1-2 NABs  
109 described by Barnes et al.<sup>3</sup> in general. The epitopes of these NABs largely overlap with  
110 RBD residues involved in the binding to ACE2. Group A and B NABs, represented by  
111 LY-CoV016 and AZD8895, respectively, usually can only bind to the 'up' RBD;  
112 whereas most of the Group C and D members, such as LY-CoV555 and REGN-10987,  
113 bind to RBDs regardless of their 'up' and 'down' conformations. Group E and F NABs  
114 are very similar to the class 3 and 4 NABs described by Barnes et al.<sup>3</sup> and target the  
115 S309/VIR-7831 site and CR3022 site, which could exhibit pan-sarbecovirus  
116 neutralization capacity (Fig 1e). Most of these NABs neutralize SARS-CoV-2 using  
117 mechanisms other than directly interfering with ACE2 binding.

118

119 Inferred from the escaping mutation profiles, various single mutations of Omicron  
120 could impair NABs of different epitope groups (Extended Data Fig. 3). Specifically,  
121 NABs in Group A-D, whose epitope overlaps with ACE2-binding motif, are largely  
122 escaped by single mutations of K417N, G446S, E484A, and Q493R. Also, a subset of  
123 NABs of Group E and F are escaped by single mutations of G339D, N440K, S371L,  
124 S375F. However, due to the extensive mutations accumulated on Omicron's RBD,

125 studying NAb's response to Omicron only in the single mutation context is insufficient.  
126 Indeed, Omicron pseudovirus neutralization and spike enzyme-linked immunosorbent  
127 assay (ELISA) showed that single mutation tolerating NAbs could also be escaped by  
128 Omicron due to multiple synergetic mutations on their epitopes (Fig 1d, Extended Data  
129 Fig. 3). In total, over 85% of the tested human NAbs are escaped, suggesting that  
130 Omicron could cause significant humoral immune evasion and potential antigenic  
131 shifting.

132  
133 It is crucial to analyze how each group of NAbs reacts to Omicron to instruct the  
134 development of NAb drugs and vaccines. Group A NAbs mainly contains the *VH3-*  
135 *53/VH3-66* germline gene-encoded antibodies, which are abundantly present in our  
136 current collection of SARS-CoV-2 neutralizing antibodies<sup>17,21,22,26,41-43</sup>, including  
137 several antibodies that have obtained emergency use authorization (CB6/LY-CoV016)  
138<sup>19</sup> or are currently being studied in clinical trials (P2C-1F11/BRII-196, BD-604/DXP-  
139 604)<sup>18,44</sup> (Fig. 2a, Extended Data Fig. 4a). Group A NAbs often exhibit less somatic  
140 mutations and shorter CDR3 length compared to other groups (Extended Data Fig. 5a,  
141 b). The epitopes of these antibodies extensively overlap with the binding site of ACE2  
142 and are often evaded by RBD mutations on K417, D420, F456, A475, L455 sites (Fig  
143 2d, Extended Data Fig. 6a,7a). Most NAbs in Group A were already escaped by B.1.351  
144 (Beta) strain (Extended Data Fig. 5d), specifically by K417N (Extended Data Fig. 8a),  
145 due to a critical salt bridge interaction between Lys417 and a negatively charged residue  
146 in the antibody (Fig. 2g). The NAbs that survived Beta strain, such as BRII-196 and  
147 DXP-604, are insensitive to the K417N single site change but could also be heavily  
148 affected by the combination of K417N and other RBD mutations located on their  
149 epitopes, like S477N, Q493R, G496S, Q498R, N501Y, and Y505H of Omicron,  
150 causing lost or reduction of neutralization (Fig 2d; Extended Data Fig. 7a).

151  
152 The *VH1-58* gene-encoded NAbs are enriched in Group B (Extended Data Fig. 4b).  
153 These NAbs such as AZD8895<sup>36</sup>, REGN-10933<sup>42</sup>, and BD-836<sup>45</sup> bind to the left  
154 shoulder of RBD, often focusing on the far tip (Fig. 2h). These NAbs are very sensitive  
155 to the change of F486, N487, and G476 (Fig 2b, Extended Data Fig. 6b). Fortunately,  
156 F486 and a few other major targeting sites of these NAbs are critically involved in  
157 ACE2-binding, and therefore they are generally harder to be escaped. A subset of NAbs  
158 in Group B, such as AZD8895 and BD-836, could survive Beta (Fig 2e); however,

159 Omicron significantly reduced Group B NABs' binding affinity to RBD, potentially  
160 through S477N/T478K/E484A on their epitope (Extended Data Fig. 7b)<sup>46</sup>, resulting in  
161 the loss of neutralization.

162

163 Group C NABs are frequently encoded by *VH1-2* and *VH1-69* (Extended Data Fig. 4c).  
164 The majority of NABs in this group could bind to both “up” and “down” RBDs,  
165 resulting in higher neutralization potency compared to other groups (Fig. 2c, Extended  
166 Data Fig. 5c). Several highly potent antibodies are found in Group C, including BD-  
167 368-2/DXP-593<sup>44</sup>, C002<sup>3</sup>, and LY-CoV555<sup>47</sup>. They bind to the right shoulder of RBD  
168 (Fig. 2i), and are mostly prone to the change of E484 (Extended Data Fig. 6c, 7c), such  
169 as the E484K mutation found in Beta (Fig. 2f). The E484A mutation seen in Omicron  
170 elicited a similar escaping effect, although the change to Ala is slightly subtler, and  
171 could be tolerated by certain antibodies in this group (Extended Data Fig. 8b). All  
172 Group C NABs tested are escaped by Omicron.

173

174 Group D NABs consist of diverse IGHV gene-encoded antibodies (Extended Data Fig.  
175 4d). Prominent members in this group include REGN-10987<sup>42</sup> and AZD1061<sup>36</sup> (Fig.  
176 3a). They further rotate down from the RBD right shoulder towards the S309 site when  
177 compared to Group C NABs (Fig. 3g). As a loop formed by residues 440-449 in RBD  
178 is critical for the targeting of this group of NABs, they are sensitive to the changes of  
179 N440, K444, G446, and N448 (Extended Data Fig. 6d, 7d). Most NABs of Group D  
180 remain active against Beta; however, G446S would substantially affect their  
181 neutralization capability against Omicron (Fig. 3d). Also, for those NABs that could  
182 tolerate G446S single mutation, the N440K/G446S combination may significantly  
183 reduce their binding affinity, resulting in that most Group D NABs are escaped by  
184 Omicron.

185

186 Group E and F NABs are rarer when compared to the other four groups. The  
187 archetypical member of each group was originally isolated from a SARS-CoV-1  
188 convalescent, and displays SARS-CoV-2 cross-neutralizing activity. There is no clear  
189 VDJ convergent effect compared to Group A, B, and C (Extended Data Fig. 4e, f), and  
190 the mutation rate and CDR3 length are larger than other groups. NABs in Group E and  
191 F rarely compete with ACE2; thus, their average half-maximal inhibitory concentration  
192 (IC50) is higher than NABs in Group A-D (Extended Data Fig. 5c). NABs in Group E,

193 such as VIR-7831/S309, may recognize a mixed protein/carbohydrate epitope,  
194 involving the N-linked glycan on N343<sup>6</sup> (Fig. 3h). Inferred from the escaping mutation  
195 profiles (Fig. 3b), Group E NAbs are often sensitive to changes of G339, T345, and  
196 R346 (Extended Data Fig 6e, 7e). The G339D mutation would affect a subset of NAbs'  
197 neutralization performance (Fig. 3e). Also, part of Group E NAbs' epitope would  
198 extend to the 440-449 loop, making them sensitive to N440K in Omicron (Fig. 3e).  
199 Noticeably, the population of Omicron with R346K is continuously increasing, which  
200 may severely affect the neutralization capacity of Group E NAbs.

201

202 Group F NAbs such as S304 target a cryptic site in RBD that is generally not exposed  
203 (Fig. 3i), therefore their neutralizing activities are generally weaker<sup>7</sup>. Group F NAbs  
204 are often sensitive to changes of F374, T376, and K378 (Extended Data Fig. 6f, 7f). A  
205 loop involving RBD residues 371-375 lies in the ridge between the E and F sites;  
206 therefore, a subset of Group F NAbs, including some Group E NAbs, could be affected  
207 by the S371L/S373P/S375F mutations if their epitopes extend to this region (Fig. 3c,  
208 f). Interestingly, a part of Group F NAbs is highly sensitive to V503 and G504, similar  
209 to the epitopes of S2X259 (Fig. 3f, j), suggesting that they can compete with ACE2.  
210 Indeed, several NAbs, such as BD55-5300 and BD55-3372, exhibit higher  
211 neutralization potency than other NAbs in Group F (Fig. 3c, 4b). However, These  
212 antibodies' neutralization capability might be undermined by N501Y and Y505H of  
213 Omicron (Fig. 3j).

214

215 As for NAb drugs, consistent with their escaping mutation profiles, the neutralization  
216 potency of LY-CoV016/LY-CoV555, REGN-10933/REGN-10987, and AZD1061 are  
217 greatly reduced by Omicron (Fig. 4a, Extended Data Fig. 9). The binding affinity of  
218 AZD8895 and BRII-196 toward Omicron RBD is also significantly reduced, likely due  
219 to multiple mutations accumulating on their epitopes, such that AZD8895 and BRII-  
220 196 failed to neutralize Omicron (Extended Data Fig. 10). BRII-198 was not tested  
221 since the antibody sequence was not released. VIR-7831 retains strong RBD binding  
222 capability, although G339 is part of its epitope, the G339D mutation in Omicron does  
223 not appear to affect VIR-7831's binding; however, VIR-7831's IC<sub>50</sub> is reduced to 181  
224 ng/mL, and may be subject to further reduction against Omicron with R346K. DXP-  
225 604's binding affinity against Omicron RBD is largely reduced compared to wildtype  
226 RBD; nevertheless, it can still neutralize Omicron at an IC<sub>50</sub> of 287 ng/mL, a nearly

227 30-fold reduction compared to wildtype (Fig. 4a). Additionally, several NABs in Group  
228 E and F have shown high potency against Omicron and broad pan-sarbecovirus  
229 neutralization ability, promising for NAB drug development (Fig. 4b). Many more  
230 NABs identified from vaccinated SARS-CoV-1 convalescents are waiting to be  
231 characterized.

232

233 The high-throughput yeast screening method provides a laboratory means for quickly  
234 examining the epitope of a certain NAB; however, the current throughput using FACS  
235 is limited and can not be used to evaluate a large NAB library. By virtue of MACS, we  
236 are able to increase the throughput by two orders of magnitude. In doing so, we were  
237 able to gain statistical confidence for the survival proportion of anti-RBD NABs in each  
238 epitope group against Omicron. The experimental accuracy for predicting the  
239 neutralization reduction for single amino acid mutations is relatively high (Extended  
240 Data Fig. 8a, b); however, current mutation screening through yeast display could not  
241 effectively probe the consequence of multiple mutations simultaneously, which  
242 requires further technical optimization.

243

244 To date, a large number of SARS-CoV-2 anti-RBD NABs have been identified from  
245 convalescents and vaccinees. The most potent NABs are frequently found in Groups A-  
246 D as we described above, which tend to directly interfere with the binding of ACE2.  
247 Nevertheless, the neutralizing powers of these NABs are often abrogated by RBD  
248 mutations in the evolutionary arms race between SARS-CoV-2 and human humoral  
249 immunity. Indeed, we showed that Omicron would escape the majority of SARS-CoV-  
250 2 NABs in this collection (Extended Data Fig. 5e). On the other hand, Groups E and F  
251 NABs are less affected by Omicron, likely because they are not abundant in population  
252 <sup>48</sup>, hence exerting less evolutionary pressure for RBD to mutate in the corresponding  
253 epitope groups. These NABs target conserved RBD regions in sarbecovirus and  
254 therefore are ideal targets for future development of pan-sarbecovirus NAB drugs.

255

## 256 **References**

- 257 1 Starr, T. N. *et al.* Prospective mapping of viral mutations that escape  
258 antibodies used to treat COVID-19. *Science* **371**, 850-854,  
259 doi:10.1126/science.abf9302 (2021).  
260 2 Starr, T. N., Greaney, A. J., Dingens, A. S. & Bloom, J. D. Complete map of  
261 SARS-CoV-2 RBD mutations that escape the monoclonal antibody LY-

- 262 CoV555 and its cocktail with LY-CoV016. *Cell Rep Med* **2**, 100255,  
263 doi:10.1016/j.xcrm.2021.100255 (2021).
- 264 3 Barnes, C. O. *et al.* SARS-CoV-2 neutralizing antibody structures inform  
265 therapeutic strategies. *Nature* **588**, 682-687, doi:10.1038/s41586-020-2852-1  
266 (2020).
- 267 4 Yuan, M. *et al.* Structural and functional ramifications of antigenic drift in  
268 recent SARS-CoV-2 variants. *Science* **373**, 818-823,  
269 doi:10.1126/science.abh1139 (2021).
- 270 5 Dejnirattisai, W. *et al.* The antigenic anatomy of SARS-CoV-2 receptor  
271 binding domain. *Cell* **184**, 2183-2200 e2122, doi:10.1016/j.cell.2021.02.032  
272 (2021).
- 273 6 Pinto, D. *et al.* Cross-neutralization of SARS-CoV-2 by a human monoclonal  
274 SARS-CoV antibody. *Nature* **583**, 290-295, doi:10.1038/s41586-020-2349-y  
275 (2020).
- 276 7 Yuan, M. *et al.* A highly conserved cryptic epitope in the receptor binding  
277 domains of SARS-CoV-2 and SARS-CoV. *Science* **368**, 630-633,  
278 doi:10.1126/science.abb7269 (2020).
- 279 8 Callaway, E. Heavily mutated Omicron variant puts scientists on alert. *Nature*  
280 **600**, 21, doi:10.1038/d41586-021-03552-w (2021).
- 281 9 Callaway, E. & Ledford, H. How bad is Omicron? What scientists know so far.  
282 *Nature*, doi:10.1038/d41586-021-03614-z (2021).
- 283 10 Li, Q. *et al.* SARS-CoV-2 501Y.V2 variants lack higher infectivity but do have  
284 immune escape. *Cell* **184**, 2362-2371 e2369, doi:10.1016/j.cell.2021.02.042  
285 (2021).
- 286 11 Cao, Y. *et al.* Humoral immune response to circulating SARS-CoV-2 variants  
287 elicited by inactivated and RBD-subunit vaccines. *Cell Res* **31**, 732-741,  
288 doi:10.1038/s41422-021-00514-9 (2021).
- 289 12 Starr, T. N. *et al.* Deep Mutational Scanning of SARS-CoV-2 Receptor  
290 Binding Domain Reveals Constraints on Folding and ACE2 Binding. *Cell* **182**,  
291 1295-1310 e1220, doi:10.1016/j.cell.2020.08.012 (2020).
- 292 13 Gu, H. *et al.* Adaptation of SARS-CoV-2 in BALB/c mice for testing vaccine  
293 efficacy. *Science* **369**, 1603-1607, doi:10.1126/science.abc4730 (2020).
- 294 14 Cerutti, G. *et al.* Potent SARS-CoV-2 neutralizing antibodies directed against  
295 spike N-terminal domain target a single supersite. *Cell Host Microbe* **29**, 819-  
296 833 e817, doi:10.1016/j.chom.2021.03.005 (2021).
- 297 15 McCallum, M. *et al.* N-terminal domain antigenic mapping reveals a site of  
298 vulnerability for SARS-CoV-2. *Cell* **184**, 2332-2347 e2316,  
299 doi:10.1016/j.cell.2021.03.028 (2021).
- 300 16 Greaney, A. J. *et al.* Complete Mapping of Mutations to the SARS-CoV-2  
301 Spike Receptor-Binding Domain that Escape Antibody Recognition. *Cell Host*  
302 *Microbe* **29**, 44-57 e49, doi:10.1016/j.chom.2020.11.007 (2021).
- 303 17 Cao, Y. *et al.* Potent Neutralizing Antibodies against SARS-CoV-2 Identified  
304 by High-Throughput Single-Cell Sequencing of Convalescent Patients' B  
305 Cells. *Cell* **182**, 73-84 e16, doi:10.1016/j.cell.2020.05.025 (2020).
- 306 18 Ju, B. *et al.* Human neutralizing antibodies elicited by SARS-CoV-2 infection.  
307 *Nature* **584**, 115-119, doi:10.1038/s41586-020-2380-z (2020).
- 308 19 Shi, R. *et al.* A human neutralizing antibody targets the receptor-binding site of  
309 SARS-CoV-2. *Nature* **584**, 120-124, doi:10.1038/s41586-020-2381-y (2020).

- 310 20 Wu, Y. *et al.* A noncompeting pair of human neutralizing antibodies block  
311 COVID-19 virus binding to its receptor ACE2. *Science* **368**, 1274-1278,  
312 doi:10.1126/science.abc2241 (2020).
- 313 21 Yuan, M. *et al.* Structural basis of a shared antibody response to SARS-CoV-2.  
314 *Science* **369**, 1119-1123, doi:10.1126/science.abd2321 (2020).
- 315 22 Robbiani, D. F. *et al.* Convergent antibody responses to SARS-CoV-2 in  
316 convalescent individuals. *Nature* **584**, 437-442, doi:10.1038/s41586-020-  
317 2456-9 (2020).
- 318 23 Liu, L. *et al.* Potent neutralizing antibodies against multiple epitopes on  
319 SARS-CoV-2 spike. *Nature* **584**, 450-456, doi:10.1038/s41586-020-2571-7  
320 (2020).
- 321 24 Baum, A. *et al.* Antibody cocktail to SARS-CoV-2 spike protein prevents rapid  
322 mutational escape seen with individual antibodies. *Science* **369**, 1014-1018,  
323 doi:10.1126/science.abd0831 (2020).
- 324 25 Brouwer, P. J. M. *et al.* Potent neutralizing antibodies from COVID-19  
325 patients define multiple targets of vulnerability. *Science* **369**, 643-650,  
326 doi:10.1126/science.abc5902 (2020).
- 327 26 Rogers, T. F. *et al.* Isolation of potent SARS-CoV-2 neutralizing antibodies  
328 and protection from disease in a small animal model. *Science* **369**, 956-963,  
329 doi:10.1126/science.abc7520 (2020).
- 330 27 Piccoli, L. *et al.* Mapping Neutralizing and Immunodominant Sites on the  
331 SARS-CoV-2 Spike Receptor-Binding Domain by Structure-Guided High-  
332 Resolution Serology. *Cell* **183**, 1024-1042 e1021,  
333 doi:10.1016/j.cell.2020.09.037 (2020).
- 334 28 Zost, S. J. *et al.* Potently neutralizing and protective human antibodies against  
335 SARS-CoV-2. *Nature* **584**, 443-449, doi:10.1038/s41586-020-2548-6 (2020).
- 336 29 Tortorici, M. A. *et al.* Ultrapotent human antibodies protect against SARS-  
337 CoV-2 challenge via multiple mechanisms. *Science* **370**, 950-957,  
338 doi:10.1126/science.abe3354 (2020).
- 339 30 Lv, Z. *et al.* Structural basis for neutralization of SARS-CoV-2 and SARS-  
340 CoV by a potent therapeutic antibody. *Science* **369**, 1505-1509,  
341 doi:10.1126/science.abc5881 (2020).
- 342 31 Zost, S. J. *et al.* Rapid isolation and profiling of a diverse panel of human  
343 monoclonal antibodies targeting the SARS-CoV-2 spike protein. *Nat Med* **26**,  
344 1422-1427, doi:10.1038/s41591-020-0998-x (2020).
- 345 32 Seydoux, E. *et al.* Analysis of a SARS-CoV-2-Infected Individual Reveals  
346 Development of Potent Neutralizing Antibodies with Limited Somatic  
347 Mutation. *Immunity* **53**, 98-105 e105, doi:10.1016/j.immuni.2020.06.001  
348 (2020).
- 349 33 Kreye, J. *et al.* A Therapeutic Non-self-reactive SARS-CoV-2 Antibody  
350 Protects from Lung Pathology in a COVID-19 Hamster Model. *Cell* **183**,  
351 1058-1069 e1019, doi:10.1016/j.cell.2020.09.049 (2020).
- 352 34 Scheid, J. F. *et al.* B cell genomics behind cross-neutralization of SARS-CoV-  
353 2 variants and SARS-CoV. *Cell* **184**, 3205-3221 e3224,  
354 doi:10.1016/j.cell.2021.04.032 (2021).
- 355 35 Tortorici, M. A. *et al.* Broad sarbecovirus neutralization by a human  
356 monoclonal antibody. *Nature* **597**, 103-108, doi:10.1038/s41586-021-03817-4  
357 (2021).

- 358 36 Dong, J. *et al.* Genetic and structural basis for SARS-CoV-2 variant  
359 neutralization by a two-antibody cocktail. *Nat Microbiol* **6**, 1233-1244,  
360 doi:10.1038/s41564-021-00972-2 (2021).
- 361 37 Starr, T. N. *et al.* SARS-CoV-2 RBD antibodies that maximize breadth and  
362 resistance to escape. *Nature* **597**, 97-102, doi:10.1038/s41586-021-03807-6  
363 (2021).
- 364 38 Martinez, D. R. *et al.* A broadly cross-reactive antibody neutralizes and  
365 protects against sarbecovirus challenge in mice. *Sci Transl Med*, eabj7125,  
366 doi:10.1126/scitranslmed.abj7125 (2021).
- 367 39 Onodera, T. *et al.* A SARS-CoV-2 antibody broadly neutralizes SARS-related  
368 coronaviruses and variants by coordinated recognition of a virus-vulnerable  
369 site. *Immunity* **54**, 2385-2398 e2310, doi:10.1016/j.immuni.2021.08.025  
370 (2021).
- 371 40 Raybould, M. I. J., Kovaltsuk, A., Marks, C. & Deane, C. M. CoV-AbDab: the  
372 coronavirus antibody database. *Bioinformatics* **37**, 734-735,  
373 doi:10.1093/bioinformatics/btaa739 (2021).
- 374 41 Barnes, C. O. *et al.* Structures of Human Antibodies Bound to SARS-CoV-2  
375 Spike Reveal Common Epitopes and Recurrent Features of Antibodies. *Cell*  
376 **182**, 828-842 e816, doi:10.1016/j.cell.2020.06.025 (2020).
- 377 42 Hansen, J. *et al.* Studies in humanized mice and convalescent humans yield a  
378 SARS-CoV-2 antibody cocktail. *Science* **369**, 1010-1014,  
379 doi:10.1126/science.abd0827 (2020).
- 380 43 Kim, S. I. *et al.* Stereotypic Neutralizing VH Clonotypes Against SARS-CoV-  
381 2 RBD in COVID-19 Patients and the Healthy Population. *bioRxiv*,  
382 2020.2006.2026.174557, doi:10.1101/2020.06.26.174557 (2020).
- 383 44 Du, S. *et al.* Structurally Resolved SARS-CoV-2 Antibody Shows High  
384 Efficacy in Severely Infected Hamsters and Provides a Potent Cocktail Pairing  
385 Strategy. *Cell* **183**, 1013-1023 e1013, doi:10.1016/j.cell.2020.09.035 (2020).
- 386 45 Du, S. *et al.* Structures of SARS-CoV-2 B.1.351 neutralizing antibodies  
387 provide insights into cocktail design against concerning variants. *Cell Res* **31**,  
388 1130-1133, doi:10.1038/s41422-021-00555-0 (2021).
- 389 46 Harvey, W. T. *et al.* SARS-CoV-2 variants, spike mutations and immune  
390 escape. *Nat Rev Microbiol* **19**, 409-424, doi:10.1038/s41579-021-00573-0  
391 (2021).
- 392 47 Jones, B. E. *et al.* The neutralizing antibody, LY-CoV555, protects against  
393 SARS-CoV-2 infection in nonhuman primates. *Sci Transl Med* **13**,  
394 doi:10.1126/scitranslmed.abf1906 (2021).
- 395 48 Tan, C. W. *et al.* Pan-Sarbecovirus Neutralizing Antibodies in BNT162b2-  
396 Immunized SARS-CoV-1 Survivors. *N Engl J Med* **385**, 1401-1406,  
397 doi:10.1056/NEJMoa2108453 (2021).

398

399

400

401

402

403

404

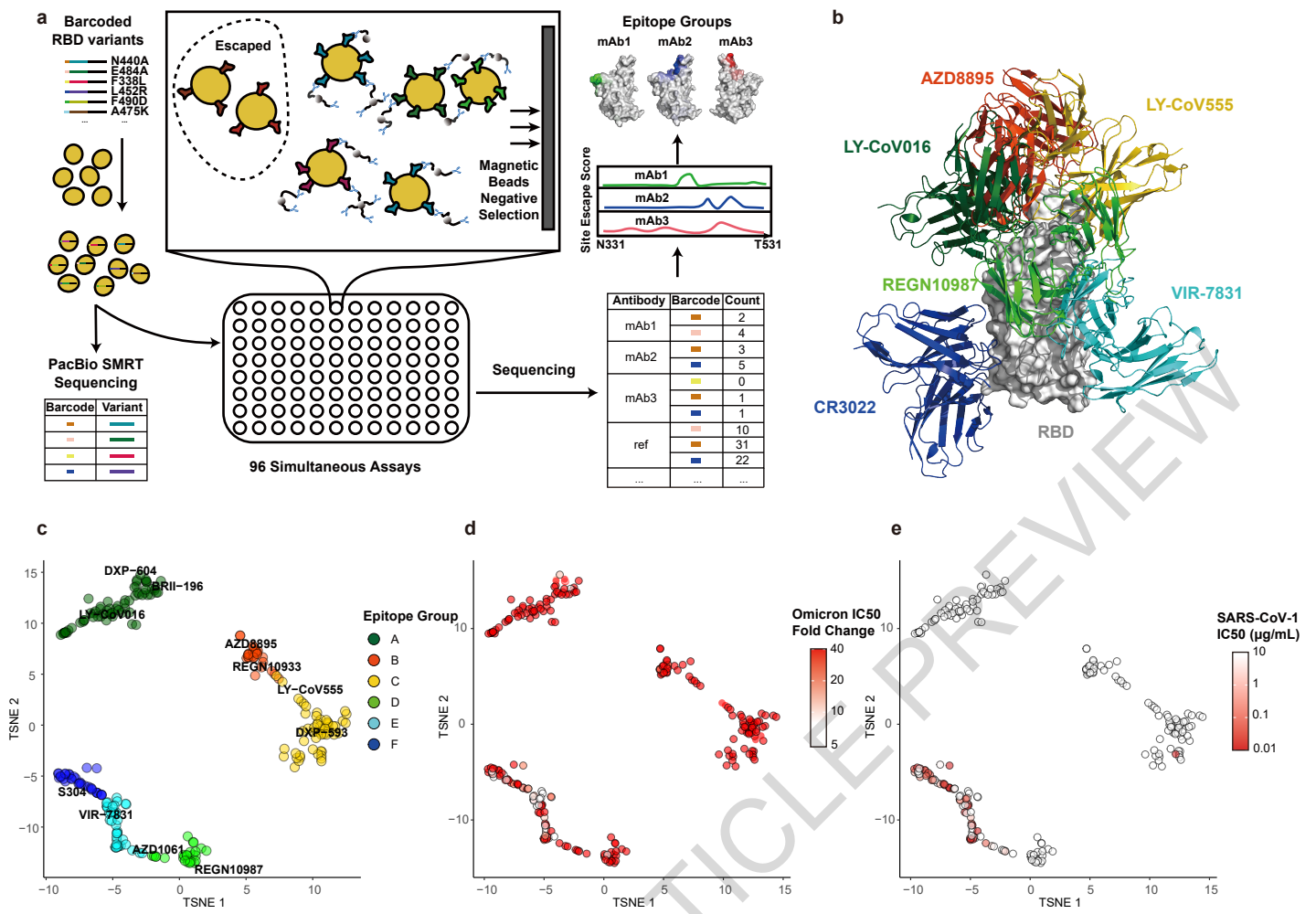


**Fig. 1**

405 **Figure legends**

406

407 **Fig. 1: Omicron greatly reduces the neutralization potency of NAbS of diverse**  
408 **epitopes.**

409 **a**, Schematic of MACS-based high-throughput yeast display mutation screening. **b**,  
410 Representative NAb structures of each epitope group. **c**, t-SNE embedding and  
411 unsupervised clustering of SARS-CoV-2 human NAbS based on each antibody  
412 escaping mutation profile. A total of 6 epitope groups (Group A-F) could be defined.  
413 **d**, Neutralization of Omicron variant (spike-pseudotyped VSV) by 247 RBD NAbS.  
414 Shades of red show IC<sub>50</sub> fold change compared with D614G of each NAb. **e**,  
415 Neutralization of SARS-CoV-1 (spike-pseudotyped VSV) by 247 RBD NAbS. Shades  
416 of red show the IC<sub>50</sub> value ( $\mu\text{g/mL}$ ) of each NAb. All pseudovirus neutralization assays  
417 are conducted in biological duplicates or triplicates.

418

419

420

421

422

423

424

425

426

427

428

429

430

431

432

433

434

435

436

437

438



439 **Fig. 2: The neutralizing abilities of Group A-C NAbs are mostly abolished by**  
440 **Omicron.**

441 **a-c**, Escaping mutation profiles of representative NAbs for group A-C, respectively.  
442 For each site, the height of a letter indicates the detected mutation escape score of its  
443 corresponding residue. Sites mutated in Omicron are highlighted. **d-f**, Heatmaps of site  
444 escape scores for NAbs of epitope group A-C, respectively. ACE2 interface residues  
445 are annotated with red blocks, and mutated sites in Omicron are marked red.  
446 Annotations on the right side of heatmaps represent pseudovirus neutralizing IC50 fold  
447 change (FC) for Omicron and Beta compared to D614G. **g-i**, Representative structures  
448 of group A-C antibodies in complex with RBD. Residues involved in important contacts  
449 are labeled. Omicron mutations are marked as blue. NAb escaping mutations (Omicron)  
450 inferred from yeast display are labeled with squares.

451

452

453

454

455

456

457

458

459

460

461

462

463

464

465

466

467

468

469

470

471

472

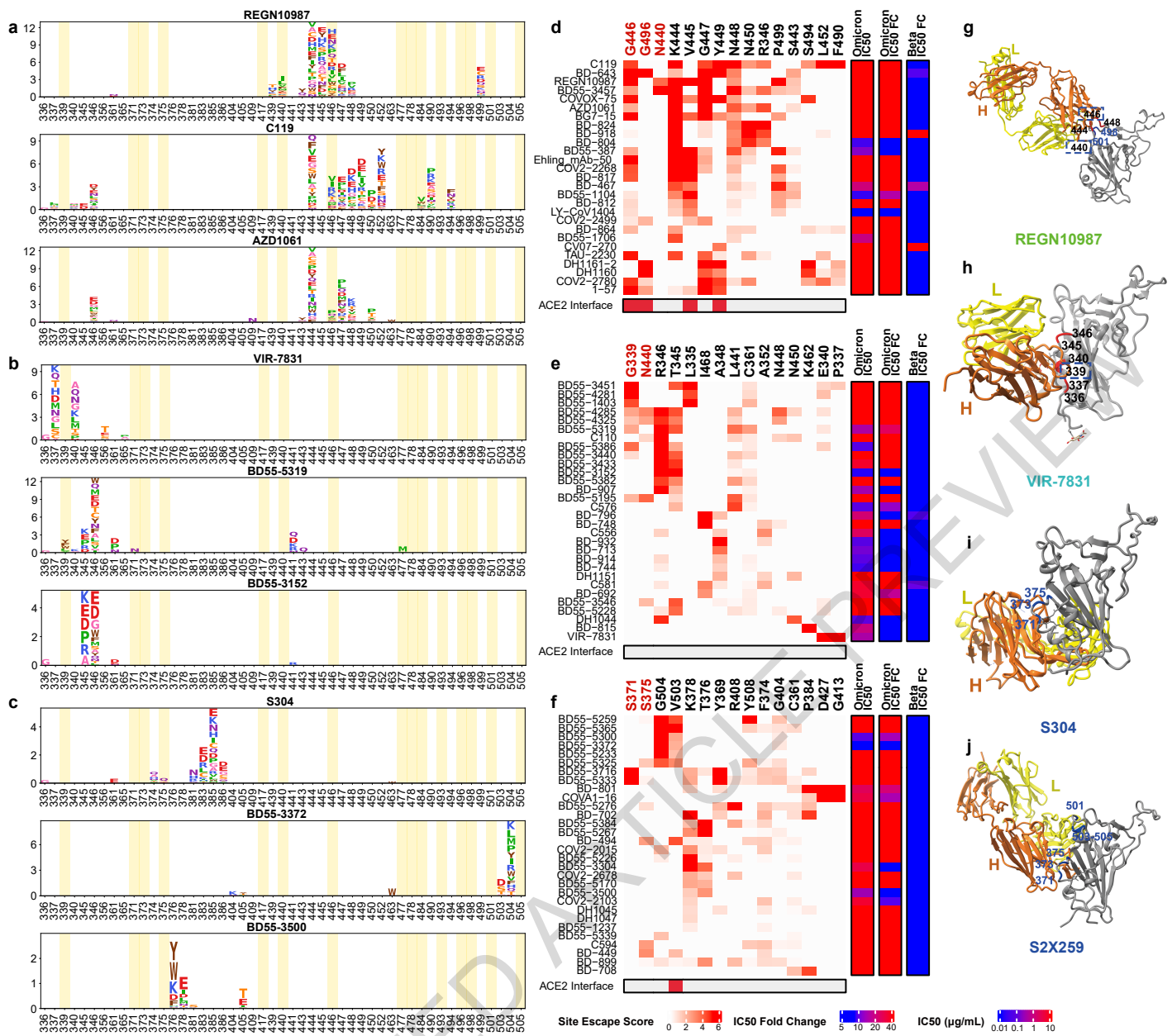


**Fig. 3**

473 **Fig. 3: The majority of Group D-E NABs are escaped by Omicron.**  
474 **a-c**, Escaping mutation profiles of representative NABs for group D-E, respectively.  
475 For each site, the height of a letter indicates the detected mutation escape score of its  
476 corresponding residue. Sites mutated in Omicron are highlighted. **d-f**, Heatmaps of site  
477 escape scores for NABs of epitope group D-E, respectively. ACE2 interface residues  
478 are annotated with red blocks, and mutated sites in Omicron are marked red.  
479 Annotations on the right side of heatmaps represent pseudovirus neutralizing IC50 fold  
480 change (FC) for Omicron and Beta compared to D614G. **g-j**, Representative structures  
481 of group D-E antibodies in complex with RBD. Residues involved in important contacts  
482 are labeled. Omicron mutations are marked as blue. NAB escaping mutations (Omicron)  
483 inferred from yeast display are labeled with squares.

484

485

486

487

488

489

490

491

492

493

494

495

496

497

498

499

500

501

502

503

504

505

506

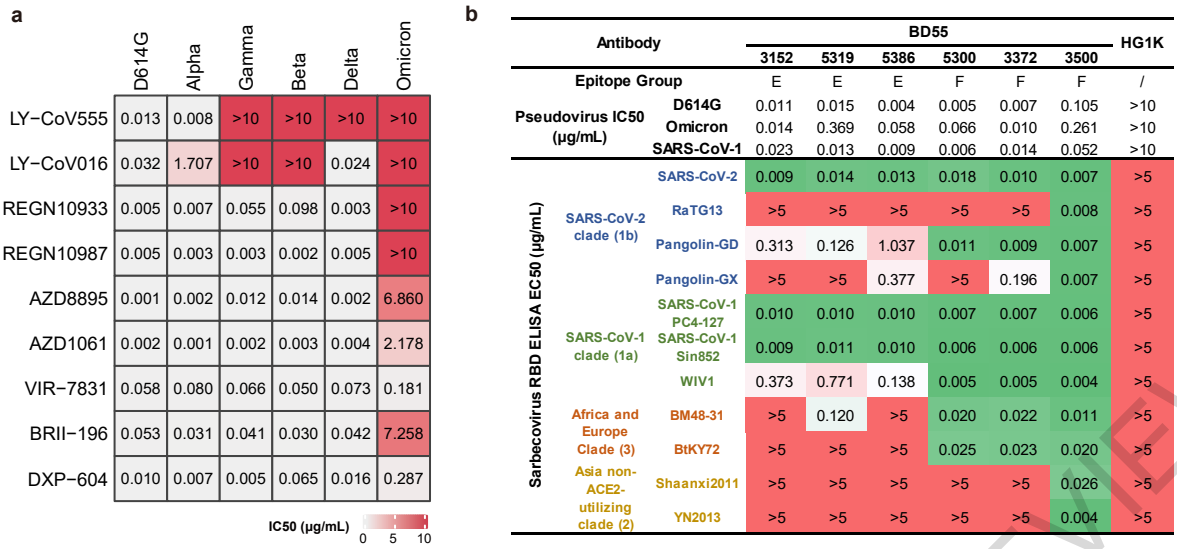


**Fig. 4**

ACCELERATED ARTICLE PREVIEW

507 **Fig. 4: Omicron escapes most NAb drugs.**

508 **a**, Neutralization of SARS-CoV-2 variants of concern (pseudotyped VSV) by 9 NAb  
509 drugs. The pseudovirus neutralization assays for every VOC were performed in  
510 biological triplicates. IC50 labeled is the average of three replicates shown in Extended  
511 Data Fig. 9. **b**, The sarbecovirus neutralization and binding capability of selected potent  
512 Omicron-neutralizing antibodies. Monoclonal antibody HG1K (IgG1 antibody against  
513 Influenza A virus subtype H7N9) was used as the negative control.

514

515

516

517

518

519

520

521

522

523

524

525

526

527

528

529

530

531

532

533

534

535

536

537

538

539

540

541 **Methods**

542

543 **Human peripheral blood mononuclear cells isolation**

544 SARS-CoV-2 convalescents, SARS-CoV-1 convalescents, and SARS-CoV-2  
545 vaccinees were recruited on the basis of prior SARS-CoV-2 infection or SARS-CoV-1  
546 infection or SARS-CoV-2 at Beijing Youan and Ditan hospital. Relevant experiments  
547 regarding SARS-CoV-2 convalescents and vaccinees were approved by the Beijing  
548 Youan Hospital Research Ethics Committee (Ethics committee archiving No. LL-2020-  
549 010-K). Relevant experiments regarding SARS-CoV-1 convalescents were approved  
550 by the Beijing Ditan Hospital Capital Medical University (Ethics committee archiving  
551 No. LL-2021-024-02). All participants provided written informed consent for the  
552 collection of information, and that their clinical samples were stored and used for  
553 research. Data generated from the research were agreed to be published. The detailed  
554 information of SARS-CoV-2 convalescents and vaccinees was previously described<sup>11</sup>.  
555 Briefly, short-term convalescents' blood samples were obtained at day 62 on average  
556 after symptoms onset. Long-term convalescents' blood samples were obtained at day  
557 371 on average after symptoms onset. No vaccination was received before blood  
558 collection. SARS-CoV-2 vaccinees' blood samples were obtained 2 weeks after  
559 complete vaccination of ZF2001 (RBD-subunit vaccine). For vaccinated SARS-CoV-  
560 1 convalescents (average age 58, n = 21), all recruited participants were previously  
561 identified for SARS-CoV-1 infection in 2003, and received two-dose vaccination of  
562 CoronaVac and a booster dose of ZF2001 with a 180-day-interval. 20mL of blood  
563 samples of the vaccinated SARS-CoV-1 convalescents were obtained 2 weeks after the  
564 booster shot. Three Healthy vaccinated donor (average age 25) were also included to  
565 serve as negative control for FACS gating. Peripheral Blood Mononuclear Cells  
566 (PBMCs) were separated from whole blood samples based on the detailed protocol  
567 described previously<sup>11</sup>. Briefly, blood samples were first diluted with 2% Fetal Bovine  
568 Serum (FBS) (Gibco) in Phosphate Buffer Saline (PBS) (Invitrogen) and subjected to  
569 Ficoll (Cytiva) gradient centrifugation. After red blood cell lysis and washing steps,  
570 PBMCs were resuspended with 2% FBS in PBS for downstream B cell isolation or 10%  
571 Dimethyl sulfoxide (Sigma-Aldrich) in FBS for further preservation.

572

573 **Antigen-specific B cell sorting and sequencing**

574 Starting with freshly isolated or thawed PBMCs, B cells were enriched by positive

575 selection using a CD19+ B cell isolation kit according to the manufacturer's  
576 instructions (STEMCELL). The enriched B cells were stained in FACS buffer (1× PBS,  
577 2% FBS, 1 mM EDTA) with the following anti-human antibodies and antigens: For  
578 every 10<sup>6</sup> cells, 3 μL FITC anti-CD19 Antibody (Biolegend, 392508), 3 μL FITC anti-  
579 CD20 Antibody (Biolegend, 302304), 3.5 μL Brilliant Violet 421 anti-CD27 Antibody  
580 (Biolegend, 302824), 3 μL PE/Cyanine7 anti-IgM(Biolegend, 314532), and  
581 fluorophore-labelled Receptor-Binding Domain (RBD) and ovalbumin (Ova) for 30  
582 min on ice. Cells were stained with 5 μL 7-AAD (eBioscience, 00-6993-50) for 10  
583 minutes before sorting. Biotinylated receptor binding domain (RBD) of SARS (Sino  
584 biological, 40634-V27H-B) or SARS-CoV-2 (Sino biological, 40592-V27H-B) were  
585 multimerized with fluorescently labeled Streptavidin (SA) for 1 hour at 4°C. RBD was  
586 mixed with SA-PE (Biolegend, 405204) and SA-APC (Biolegend, 405207) at a 4:1  
587 molar ratio. For every 10<sup>6</sup> cells, 6 ng SA was used to stain. Single CD19 or CD20+,  
588 CD27+, IgM-, Ova-, RBD-PE+, RBD-APC+, live B cells were sorted on an Astrios EQ  
589 (BeckMan Coulter) into PBS containing 30% FBS (Supplementary Data 2). FACS  
590 sorting were controlled by Summit 6.0 (Beckman Coulter). FACS data analyses were  
591 done by FlowJo 10.8. Cells obtained after FACS were sent for 5'-mRNA and V(D)J  
592 libraries preparation as previously described<sup>11</sup>, which were further submitted to  
593 Illumina sequencing on a Hiseq 2500 platform, with the 26x91 pair-end reading mode.

594

### 595 **V(D)J sequence data analysis**

596 The raw FASTQ files were processed by Cell Ranger (version 6.1.1) pipeline using  
597 GRCh38 reference. Sequences were generated using "cellranger multi" or "cellranger  
598 vdj" with default parameters. Antibody sequences were processed by  
599 IMGT/DomainGapAlign (version 4.10.2) to obtain the annotations of V(D)J, regions  
600 of complementarity determining regions (CDR), and the mutation frequency<sup>49,50</sup>.  
601 Mutation count divided by the length of the V gene peptide is defined as the amino acid  
602 mutation rate of the V gene.

603

### 604 **Recombinant antibody production**

605 Paired immunoglobulin heavy and light chain genes obtained from 10X Genomics  
606 V(D)J sequencing and analysis were submitted to recombinant monoclonal antibody  
607 synthesis. Briefly, heavy and light genes were cloned into expression vectors,

608 respectively, based on Gibson assembly, and subsequently co-transfected into  
609 HEK293F cells (ThermoFisher, R79007). The secreted monoclonal antibodies from  
610 cultured cells were purified by protein A affinity chromatography. The specificities of  
611 these antibodies were determined by ELISA.

612

### 613 **ELISA**

614 ELISA plates were coated with RBD (SARS-CoV-2 WT, SARS-CoV-2 Omicron,  
615 SARS-CoV-1 RBD, Sino Biological Inc.) at 0.03 µg/mL and 1 µg/mL in PBS at 4°C  
616 overnight. After standard washing and blocking, 100 µL 1µg/mL antibodies were added  
617 to each well. After a 2 h incubation at room temperature, plates were washed and  
618 incubated with 0.08 µg/mL goat anti-human IgG (H+L)/HRP (JACKSON, 109-035-  
619 003) for 1 h incubation at room temperature. Tetramethylbenzidine (TMB) (Solarbio)  
620 was then added, and the reaction was stopped by adding H<sub>2</sub>SO<sub>4</sub>. OD450 was measured  
621 by an ELISA microplate reader. An antibody is defined as ELISA-positive when the  
622 OD450 (1 µg/mL RBD) is three times larger than the negative control, which utilizes  
623 an H7N9 specific human IgG1 antibody (HG1K, Sino Biology Cat #HG1K).

624

### 625 **Pseudovirus neutralization assay**

626 Pseudovirus neutralization assay was performed to evaluate neutralizing ability of  
627 antibodies. The detailed process was previously described by Cao et al.<sup>12</sup>. Briefly,  
628 serially diluted antibodies were first incubated with pseudotyped virus for 1h, and the  
629 mixture was then incubated with Huh-7 cells. After 24h incubation in an incubator at  
630 37°C, cells were collected and lysed with luciferase substrate (PerkinElmer), then  
631 proceeded to luminescence intensity measurement by a microplate reader. IC50 was  
632 determined by a four-parameter non-linear regression model using PRISM (v9.0.1).  
633 Omicron pseudovirus contains the following mutations: A67V, H69del, V70del, T95I,  
634 G142D, V143del, Y144del, Y145del, N211del, L212I, ins214EPE, G339D, S371L,  
635 S373P, S375F, K417N, N440K, G446S, S477N, T478K, E484A, Q493R, G496S,  
636 Q498R, N501Y, Y505H, T547K, D614G, H655Y, N679K, P681H, N764K, D796Y,  
637 N856K, Q954H, N969K, L981F.

638

### 639 **Biolayer interferometry**

640 Biolayer interferometry assays were conducted on Octet® R8 Protein Analysis System

641 (Fortebio) following the manufacturer's instruction. Briefly, after baseline calibration,  
642 Protein A biosensors (Fortebio) were immersed with antibodies to capture the antibody,  
643 then sensors were immersed in PBS with 0.05% Tween-20 to the baseline. After  
644 association with different concentrations of RBD of SARS-CoV-2 variants (Omicron  
645 RBD: 40592-V08H85), disassociation was conducted. Data were recorded using Octet  
646 BLI Discovery (12.2) and analyzed using Octet BLI Analysis (12.2).

647

### 648 **RBD Deep Mutational Scanning Library construction**

649 The yeast-display RBD mutant libraries used here were constructed as described by  
650 Starr et al.,<sup>12</sup> based on the spike receptor-binding domain (RBD) from SARS-CoV-2  
651 (NCBI GenBank: MN908947, residues N331-T531) with the modifications that instead  
652 of 16-nucleotide barcode (N16), a unique 26-nucleotide (N26), barcode was appended  
653 to each RBD variant as an identifier in order to decrease sequencing cost by eliminating  
654 the use of PhiX. Briefly, three rounds of mutagenesis PCR were performed with  
655 designed and synthesized mutagenetic primer pools; in order to solid our conclusion,  
656 we constructed two RBD mutant libraries independently. RBD mutant libraries were  
657 then cloned into pETcon 2649 vector and the assembled products were electroporated  
658 into electrocompetent DH10B cells to enlarge plasmid yield. Plasmid extracted from *E.*  
659 *coli* were transformed into the EBY100 strain of *Saccharomyces cerevisiae* via the  
660 method described by Gietz and Schiestl<sup>51</sup>. Transformed yeast population were screened  
661 on SD-CAA selective plate and further cultured in SD-CAA liquid medium at a large  
662 scale. The resulted yeast libraries were flash frozen by liquid nitrogen and preserved at  
663 -80°C.

664

### 665 **PacBio library preparation, sequencing, and analysis**

666 The correspondence of RBD gene sequence in mutant library and N26 barcode was  
667 obtained by PacBio sequencing. Firstly, the bacterially-extracted plasmid pools were  
668 digested by NotI restriction enzyme and purified by agarose gel electrophoresis, then  
669 proceed to SMRTbell ligation. Four RBD mutant libraries were sequenced in one  
670 SMRT cell on a PacBio Sequel II platform. PacBio SMRT sequencing subreads were  
671 converted to HiFi ccs reads with pbccs, and then processed with a slightly modified  
672 version of the script previously described<sup>12</sup> to generate the barcode-variant dictionary.  
673 To reduce noise, variants containing stop codons or supported by only one ccs read

674 were removed from the dictionary and ignored during further analysis.

675

### 676 **Magnetic-activated cell sorting (MACS)-based mutation escape profiling**

677 ACE2 binding mutants were sorted based on magnetic beads to eliminate non-  
678 functional RBD variants. Briefly, the biotin binder beads (Thermo Fisher) were washed  
679 and prepared as the manufacturer's instruction and incubated with biotinylated ACE2  
680 protein (Sino Biological Inc.) at room temperature with mild rotation. The ACE2 bound  
681 beads were washed twice and resuspend with 0.1% BSA buffer (PBS supplemented  
682 with 0.1% bovine serum albumin), and ready for ACE2 positive selection. Transformed  
683 yeast library were inoculated into SD-CAA and grown at 30°C with shaking for 16-  
684 18h, then back-diluted into SG-CAA at 23°C with shaking to induce RBD surface  
685 expression. Yeasts were collected and washed twice with 0.1% BSA buffer and  
686 incubated with aforementioned ACE2 bound beads at room temperature for 30min with  
687 mild rotating. Then, the bead-bound cells were washed, resuspend with SD-CAA  
688 media, and grown at 30°C with shaking. After overnight growth, the bead-unbound  
689 yeasts were separated with a magnet and cultured in a large scale. The above ACE2  
690 positive selected yeast libraries were preserved at -80°C in aliquots as a seed bank for  
691 antibody escape mapping.

692

693 One aliquot of ACE2 positive selected RBD library was thawed and inoculated into  
694 SD-CAA, then grown at 30°C with shaking for 16-18h. 120 OD units were back-diluted  
695 into SG-CAA media and induced for RBD surface expression. Two rounds of  
696 sequential negative selection to sort yeast cells that escape Protein A conjugated  
697 antibody binding were performed according to the manufacturer's protocol. Briefly,  
698 Protein A magnetic beads (Thermo Fisher) were washed and resuspend in PBST (PBS  
699 with 0.02% Tween-20). Then beads were incubated with neutralizing antibody and  
700 rotated at room temperature for 30min. The antibody-conjugated beads were washed  
701 and resuspend in PBST. Induced yeast libraries were washed and incubated with  
702 antibody-conjugated beads for 30min at room temperature with agitation. The  
703 supernatant was separated and proceed to a second round of negative selection to ensure  
704 full depletion of antibody-binding yeast.

705

706 To eliminate yeast that did not express RBD, MYC-tag based RBD positive selection

707 was conducted according to the manufacturer's protocol. First, anti-c-Myc magnetic  
708 beads (Thermo Fisher) were washed and resuspend with 1X TBST (TBS with Tween-  
709 20), then the prepared beads were incubated for 30min with the antibody escaping  
710 yeasts after two rounds of negative selection. Yeasts bound by anti-c-Myc magnetic  
711 beads were wash with 1X TBST and grown overnight in SD-CAA to expand yeast  
712 population prior to plasmid extraction.

713

714 Overnight cultures of MACS sorted antibody-escaped and ACE2 preselected yeast  
715 populations were proceed to yeast plasmid extraction kit (Zymo Research). PCRs were  
716 performed to amplify the N26 barcode sequences as previously described<sup>13</sup>. The PCR  
717 products were purified with 0.9X Ampure XP beads (Beckman Coulter) and submitted  
718 to 75bp single-end Illumina Nextseq 500 sequencing.

719

## 720 **Deep mutational scanning data processing**

721

722 Raw single-end Illumina sequencing reads were trimmed and aligned to the reference  
723 barcode-variant dictionary generated as described above to get the count of each variant  
724 with *dms\_variants* Python package (version 0.8.9). For libraries with N26 barcodes, we  
725 slightly modified the *illuminabarcodeparser* class of this package to tolerate one low  
726 sequencing quality base in the barcode region. The escape score of variant X is defined  
727 as  $F \times (n_{X,ab} / N_{ab}) / (n_{X,ref} / N_{ref})$ , where  $n_{X,ab}$  and  $n_{X,ref}$  is the number of detected barcodes  
728 for variant X,  $N_{ab}$  and  $N_{ref}$  are the total number of barcodes in antibody-selected (ab)  
729 library and reference (ref) library respectively as described by Starr et al.<sup>12</sup>. Different  
730 from FACS experiments, as we couldn't measure the number of cells retained after  
731 MACS selection precisely, here F is considered as a scaling factor to transform raw  
732 escape fraction ratios to 0-1 range, and is calculated from the first and 99th percentiles  
733 of raw escape fraction ratios. Scores less than the first percentile or larger than the 99th  
734 percentile are considered to be outliers and set to zero or one, respectively. For each  
735 experiment, barcodes detected by <6 reads in the reference library were removed to  
736 reduce the impact of sampling noise, and variants with ACE2 binding below -2.35 or  
737 RBD expression below -1 were removed as previously described<sup>12</sup>. Finally, we built  
738 global epistasis models with *dms\_variants* package for each library to estimate single  
739 mutation escape scores, utilizing the Python scripts provided by Greaney et al.<sup>16</sup>. To  
740 reduce experiment noise, sites are retained for further analysis only if its total escape

741 score is at least 0.01, and at least 3 times greater than the median score of all sites. For  
742 antibodies measured by 2 independent experiments, only sites which pass the filter in  
743 both experiments are retained. Logo plots in Fig. 2, Fig. 3, Extended Data Fig. 2 and  
744 Supplementary Data 1 are generated by Python package *logomaker* (version 0.8).

745

## 746 **Antibody clustering**

747 Antibody clustering and epitope group identification were performed based on the  
748  $N \times M$  escape score matrix, where  $N$  is the number of antibodies which pass the quality  
749 controlling filters, and  $M$  is the number of informative sites on SARS-CoV-2 RBD.  
750 Each entry of the matrix  $A_{nm}$  refers to the total escape score of all kinds of mutations  
751 on site  $m$  of antibody  $n$ . The dissimilarity between two antibodies is defined based on  
752 the Pearson's correlation coefficient of their escape score vectors, i. e.  $D_{ij} = 1 -$   
753  $\text{Corr}(\mathbf{A}_i, \mathbf{A}_j)$ , where  $\text{Corr}(\mathbf{A}_i, \mathbf{A}_j) = \mathbf{x}_i \cdot \mathbf{x}_j / |\mathbf{x}_i| |\mathbf{x}_j|$  and vector  $\mathbf{x}_i = \mathbf{A}_i - \text{Mean}(\mathbf{A}_i)$ . Sites with at  
754 least 6 escaped antibodies (site escape score  $> 1$ ) were considered informative and  
755 selected for dimensionality reduction and clustering. We utilized R function *cmdscale*  
756 to convert the cleaned escape matrix into an  $N \times 6$  feature matrix by multidimensional  
757 scaling (MDS) with the dissimilarity metric described above, followed by unsupervised  
758 k-medoids clustering within this 6-dimensional antibody feature space, using *pam*  
759 function of R package *cluster* (version 2.1.1). Finally, two-dimensional t-Distributed  
760 Stochastic Neighbor Embedding (tSNE) embeddings were generated with *Rtsne*  
761 package (version 0.15) for visualization. 2D t-SNE plots are generated by *ggplot2*  
762 (version 3.3.3), and heatmaps are generated by *ComplexHeatmap* package (version  
763 2.6.2).

764

## 765 **Reference**

- 766 49 Ehrenmann, F., Kaas, Q. & Lefranc, M. P. IMGT/3Dstructure-DB and  
767 IMGT/DomainGapAlign: a database and a tool for immunoglobulins or  
768 antibodies, T cell receptors, MHC, IgSF and MhcSF. *Nucleic Acids Res* **38**,  
769 D301-307, doi:10.1093/nar/gkp946 (2010).
- 770 50 Ehrenmann, F. & Lefranc, M. P. IMGT/DomainGapAlign: IMGT standardized  
771 analysis of amino acid sequences of variable, constant, and groove domains  
772 (IG, TR, MH, IgSF, MhSF). *Cold Spring Harb Protoc* **2011**, 737-749,  
773 doi:10.1101/pdb.prot5636 (2011).
- 774 51 Gietz, R. D. & Schiestl, R. H. High-efficiency yeast transformation using the  
775 LiAc/SS carrier DNA/PEG method. *Nat Protoc* **2**, 31-34,  
776 doi:10.1038/nprot.2007.13 (2007).

777

778

779 **Acknowledgments**

780 We thank Professor Jesse Bloom for his generous gift of the yeast SARS-CoV-2 RBD  
781 libraries. We thank Beijing BerryGenomics for the help on DNA sequencing. We thank  
782 Sino Biological Inc. for the technical assistance on mAbs and Omicron RBD  
783 expression. We thank Sartorius (Shanghai) Trading Co., Ltd. for providing instrumental  
784 help with BLI measurement. We thank Jia Luo and Hongxia Lv (National Center for  
785 Protein Sciences and core facilities at School of Life Sciences at Peking University) for  
786 the help in flow cytometry. This project is financially supported by the Ministry of  
787 Science and Technology of China (CPL-1233).

788

789 **Author contributions**

790 Y.C. and X.S.X designed the study. Y.C. and F.S coordinated the characterizations of  
791 the NAbs. J.W., F.J., H.L., H.S. performed and analyzed the yeast display mutation  
792 screening experiments. T.X., W.J., X.Y., P.W., H.L. performed the pseudovirus  
793 neutralization assays. W.H., Q.L., T.L., Y.Y., Q.C., S.L., Y.W. prepared the VSV-based  
794 SARS-CoV-2 pseudovirus. A.Y., Y.W., S.Y., R.A., W.S. performed and analyzed the  
795 antigen-specific single B cell VDJ sequencing. X.N., R.A. performed the antibody BLI  
796 studies. Z.C., S.D., P.L., L.W., Z.Z., X.W., J.X. performed the antibody structural  
797 analyses. P.W., Y.W., J.W, H.S, H.L. performed the ELISA experiments. X.H. and R.J.  
798 coordinated the blood samples of vaccinated SARS-CoV-1 convalescents. Y.C., X.W.,  
799 J.X., X.S.X wrote the manuscript with inputs from all authors.

800

801 **Declaration of interests**

802 X.S.X. and Y.C. are listed as inventors on a patent related to BD series antibodies and  
803 DXP-604 (PCT/CN2021/093305). X.S.X. and Y.C. are founders of Singlomics  
804 Biopharmaceuticals Inc. Other authors declare no competing interests.

805

806 **Corresponding authors**

807 Correspondence to Yunlong Cao or Xiangxi Wang or Junyu Xiao or Youchun Wang or  
808 Xiaoliang Sunney Xie. Request for materials described in this study should be directed  
809 to Xiaoliang Sunney Xie.

810

811 **Data availability**

812 Data availability Processed escape maps for NAbs are available in Supplementary Data  
813 1 (as figures), or at <https://github.com/sunneyxielab/SARS-CoV-2-RBD-Abs-HTDMS>  
814 (as mutation escape score data). Raw Illumina and PacBio sequencing data are available  
815 on NCBI Sequence Read Archive BioProject PRJNA787091. We used  
816 vdj\_GRCh38\_alts\_ensembl-5.0.0 as the reference of V(D)J alignment, which can be  
817 obtained from

818 <https://support.10xgenomics.com/single-cell-vdj/software/downloads/latest>.

819 IMGT/DomainGapAlign is based on the built-in latest IMGT antibody database, and  
820 we let the "Species" parameter as "Homo sapiens" while kept the others as default.

821 FACS-based deep mutational scanning datasets could be downloaded from  
822 [https://media.githubusercontent.com/media/jbloombloomlab/SARS2\\_RBD\\_Ab\\_escape\\_map](https://media.githubusercontent.com/media/jbloombloomlab/SARS2_RBD_Ab_escape_map)  
823 [s/main/processed\\_data/escape\\_data.csv](https://media.githubusercontent.com/media/jbloombloomlab/SARS2_RBD_Ab_escape_map).

824 Processed data of this study has been added to this repository as well.

825

#### 826 **Code availability**

827 Scripts for analyzing SARS-CoV-2 escaping mutation profile data and for reproducing  
828 figures in this paper are available at [https://github.com/sunneyxielab/SARS-CoV-2-](https://github.com/sunneyxielab/SARS-CoV-2-RBD-Abs-HTDMS)  
829 [RBD-Abs-HTDMS](https://github.com/sunneyxielab/SARS-CoV-2-RBD-Abs-HTDMS).

830

831

832

833

834

835

836

837

838

839

840

841

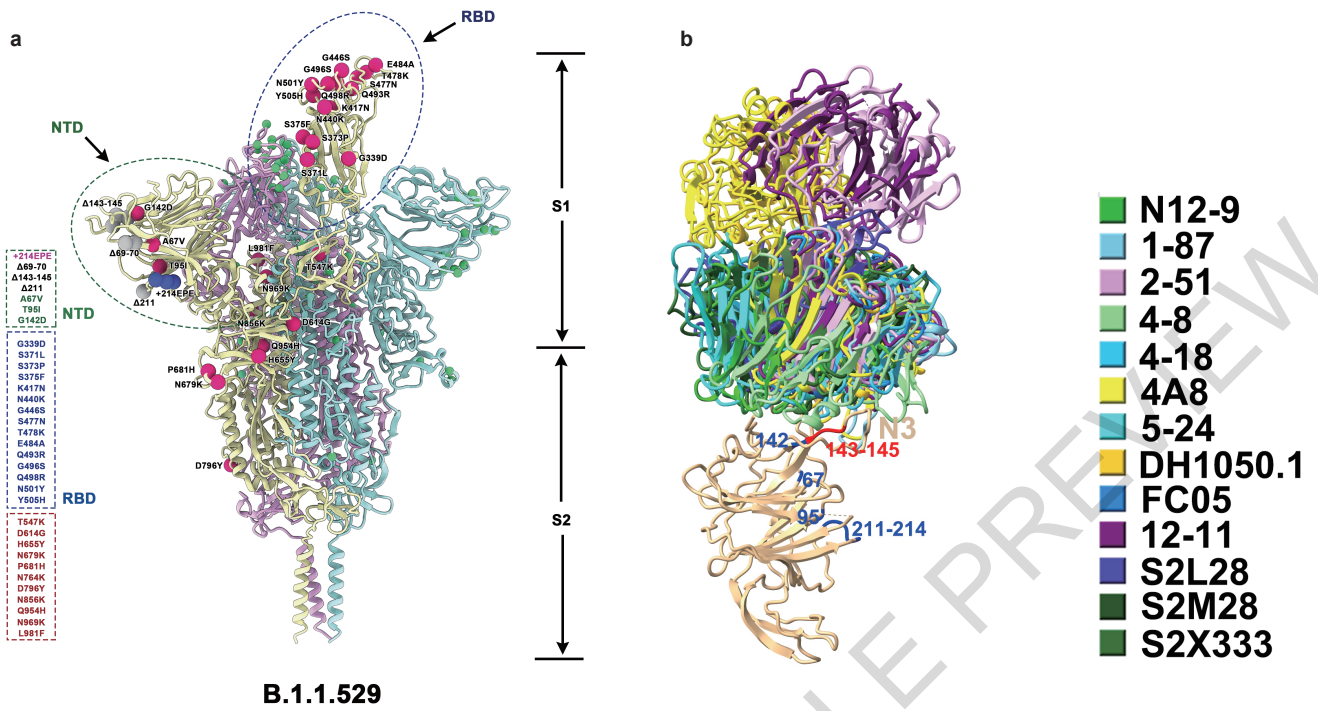
842

843

844

845

Extended Data Fig. 1



ACCELERATED ARTICLE PREVIEW

846 **Extended Data Fig. 1: Illustration of SARS-CoV-2 spike with Omicron's**  
847 **mutations.**

848 **a**, SARS-CoV-2 D614G spike protein structure overlaid with Omicron mutations.  
849 Omicron's (BA.1) popular mutations are marked by red (for substitutions), blue (for  
850 insertions) and gray balls (for deletions). **b**, NTD-binding NAbs shown together in  
851 complex with NTD. Substitutions and deletions of Omicron NTD are colored blue and  
852 red, respectively.

853

854

855

856

857

858

859

860

861

862

863

864

865

866

867

868

869

870

871

872

873

874

875

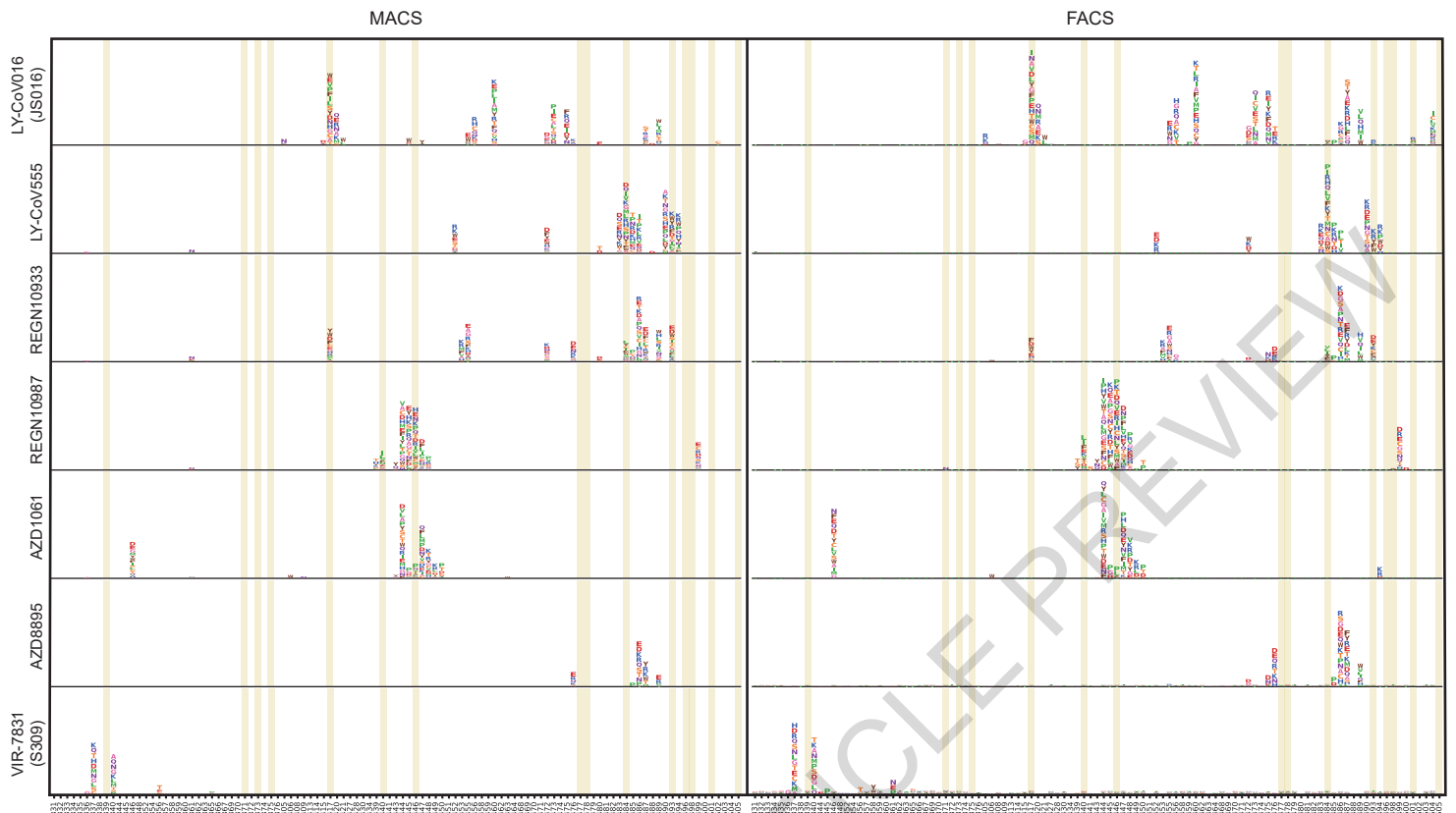
876

877

878

879

# Extended Data Fig. 2



880 **Extended Data Fig. 2: Comparison between FACS and MACS-based deep**  
881 **mutational scanning.**

882 Deep mutational scanning maps with MACS-based (left) and FACS-based assays  
883 (right) of seven therapeutic neutralizing antibodies that have received emergency use  
884 authorization. Sites mutated in the Omicron variant are highlighted. Mutation amino  
885 acids of each site are shown by single letters. The heights represent mutation escape  
886 score, and colors represent chemical properties. FACS-based data were obtained from  
887 public datasets by Jesse Bloom.

888

889

890

891

892

893

894

895

896

897

898

899

900

901

902

903

904

905

906

907

908

909

910

911

912

913



914 **Extended Data Fig. 3: Omicron neutralization IC50 fold-change distribution of**  
915 **247 NAbs of diverse epitopes.**

916 Fold-change of IC50 (VSV pseudovirus neutralization) compared to D614G by Beta  
917 and Omicron (BA.1) are shown for all 247 NAbs tested. The impact of each RBD  
918 mutation of Omicron on NAbs' binding is inferred from yeast display mutation  
919 screening. Each NAb's binding to Omicron RBD was validated through ELISA. All  
920 neutralization and ELISA assays were conducted in biological duplicates.

921

922

923

924

925

926

927

928

929

930

931

932

933

934

935

936

937

938

939

940

941

942

943

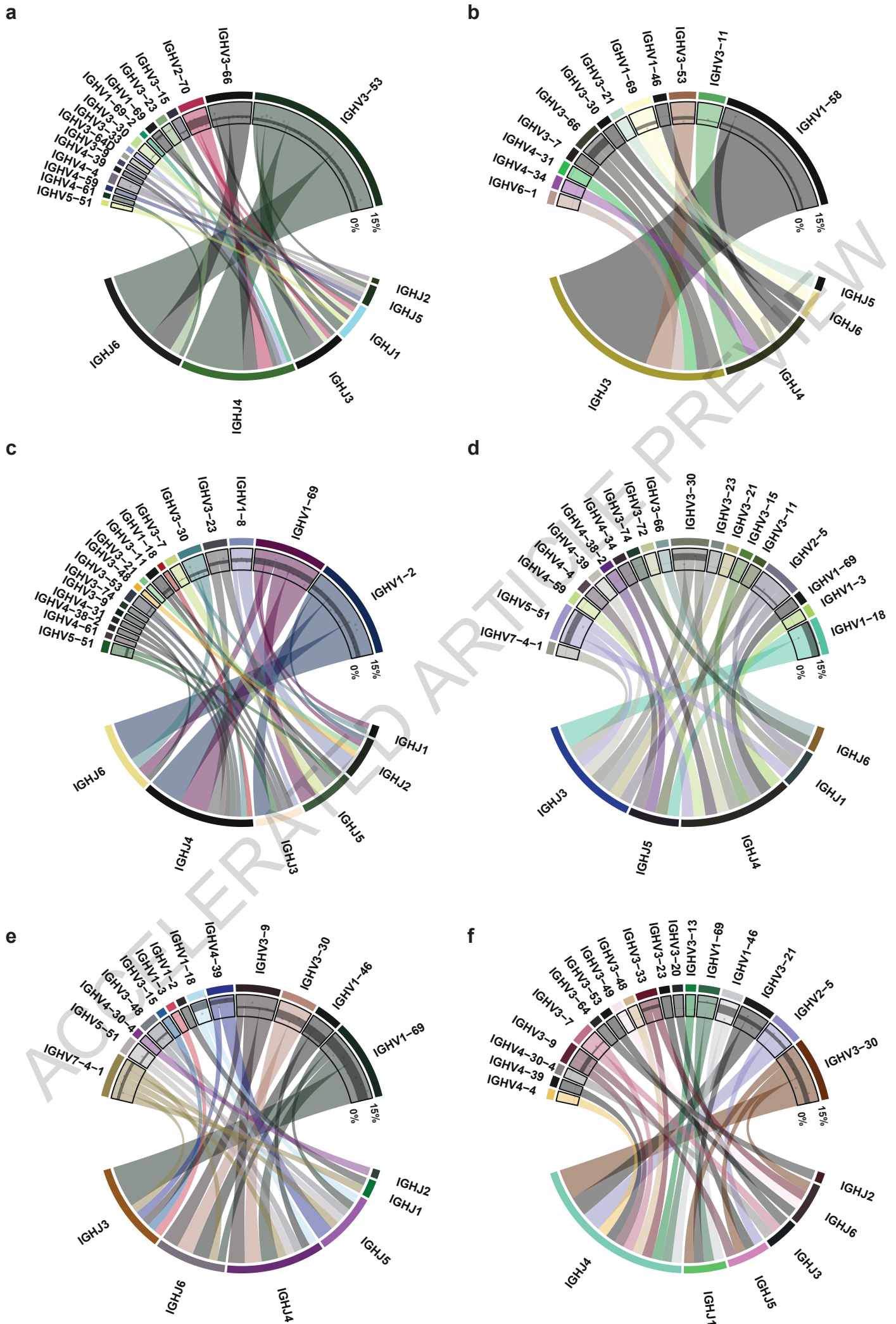
944

945

946

947

# Extended Data Fig. 4



948 **Extended Data Fig. 4: Heavy chain V/J segment recombination of NAbs of each**  
949 **epitope group.**

950 **a-f**, Chord diagrams showing the heavy chain V segment and J segment recombination  
951 of epitope group A(a), B(b), C(c), D(d), E(e) and F(f). The width of the arc linking a V  
952 segment to a J segment indicates the antibody number of the corresponding  
953 recombination. The inner layer scatter plots show the V segment amino acid mutation  
954 rate, while black strips show the 25%~75% quantile of mutation rates.

955

956

957

958

959

960

961

962

963

964

965

966

967

968

969

970

971

972

973

974

975

976

977

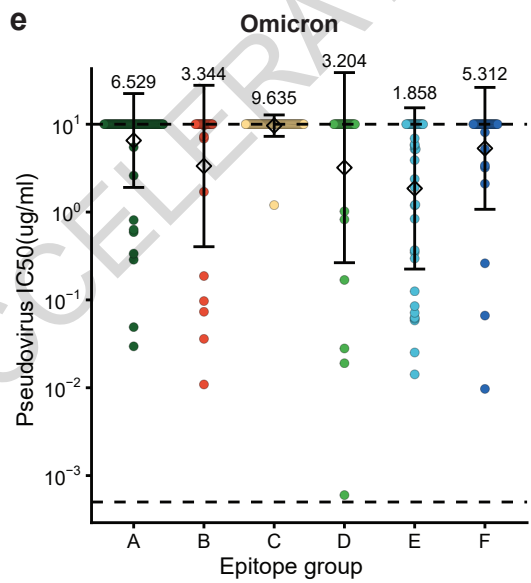
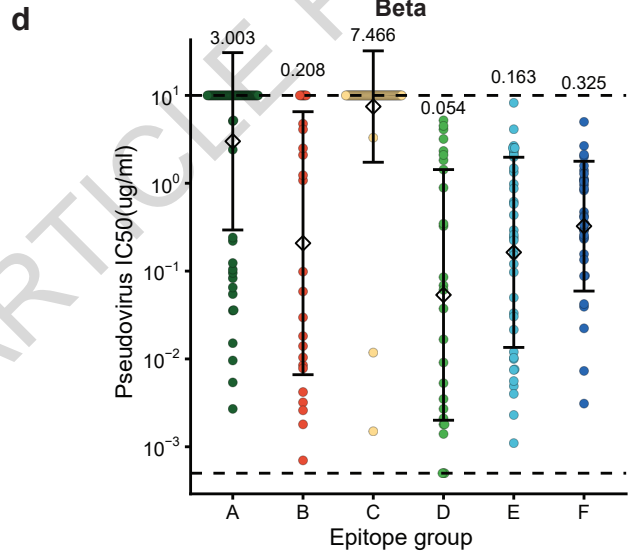
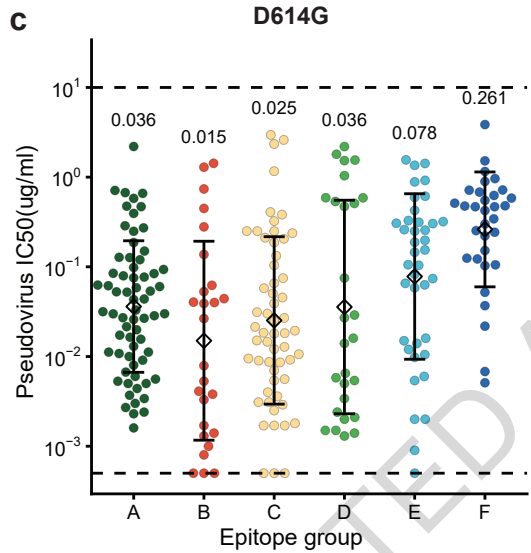
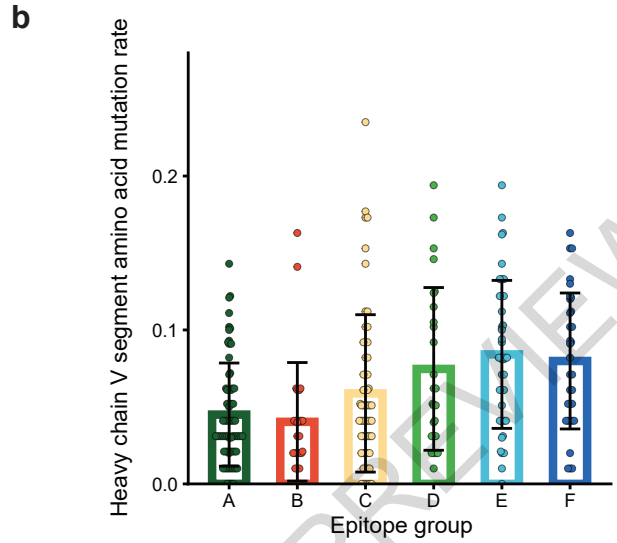
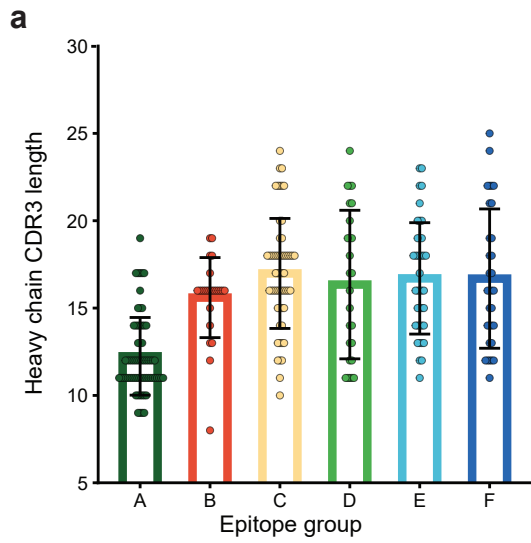
978

979

980

981

Extended Data Fig. 5



982 **Extended Data Fig. 5. Neutralization potency, heavy chain CDR3 length, and**  
983 **mutation rate distribution for NABs of each epitope group.**

984 **a**, The length of H chain complementarity-determining region 3 (HCDR3) amino acid  
985 sequence for NABs in each epitope group (n=66, 26, 57, 27, 39, 32 antibodies for  
986 epitope group A, B, C, D, E, F, respectively). HCDR3 lengths are displayed as mean  $\pm$   
987 s.d. **b**, The V segment amino acid mutation rate for NABs in each epitope group (n=66,  
988 26, 57, 27, 39, 32 antibodies for epitope group A, B, C, D, E, F, respectively). Mutation  
989 rates are calculated are displayed as mean  $\pm$  s.d. **c-e**, The IC50 against D614G(c),  
990 Beta(d), and Omicron(e) variants for NABs in each epitope group (n=66, 26, 57, 27, 39,  
991 32 antibodies for epitope group A, B, C, D, E, F, respectively). IC50 values are  
992 displayed as mean  $\pm$  s.d. in the log10 scale. Pseudovirus assays for each variant are  
993 biologically replicated twice. Dotted lines show the detection limit, which is from  
994 0.0005  $\mu$ g/mL to 10  $\mu$ g/mL. IC50 geometric means are also labeled on the figure.

995

996

997

998

999

1000

1001

1002

1003

1004

1005

1006

1007

1008

1009

1010

1011

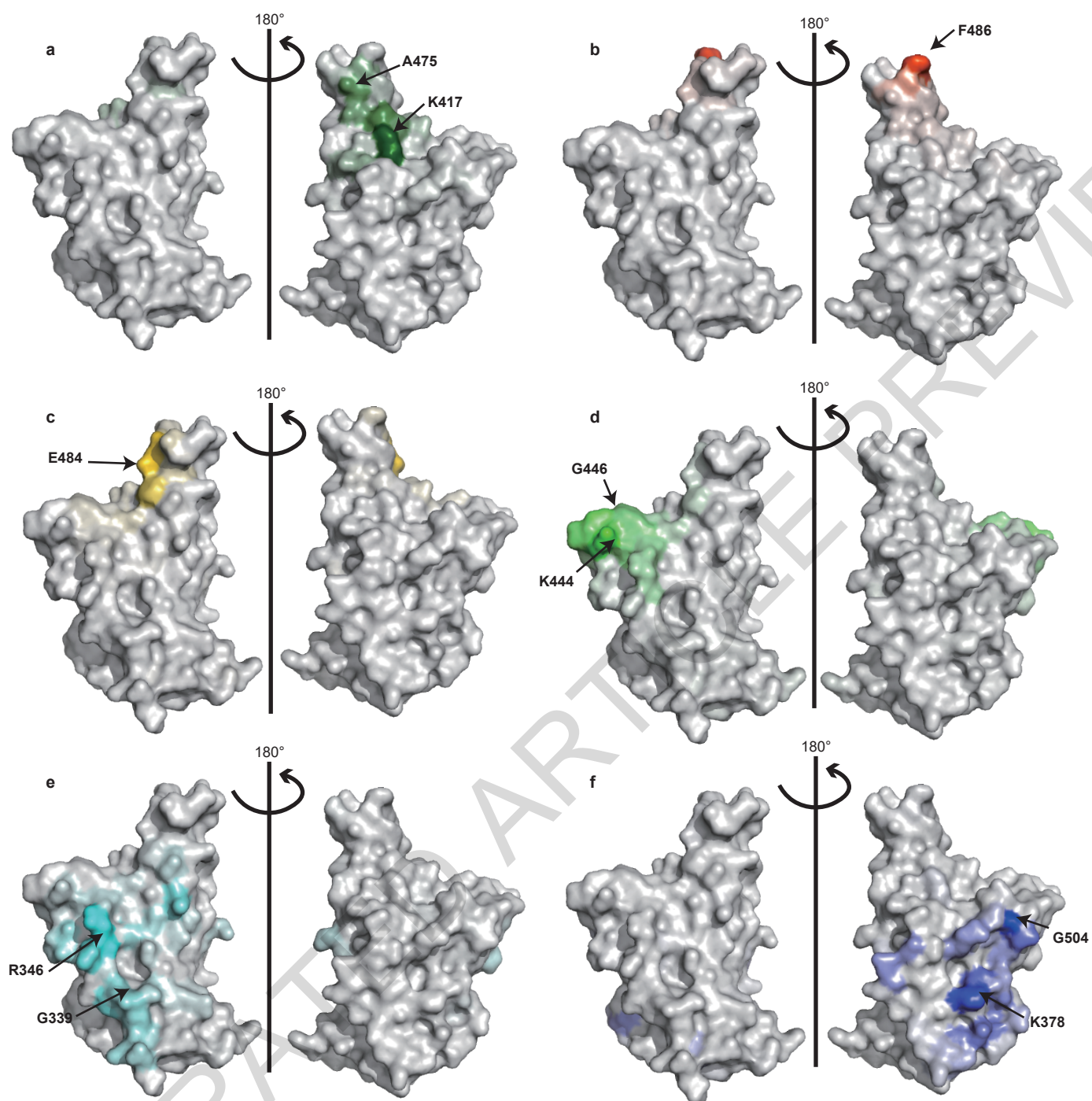
1012

1013

1014

1015

Extended Data Fig. 6



1016 **Extended Data Fig. 6: Escape hotspots of different epitope groups on the RBD**  
1017 **surface.**

1018 **a-f**, Aggregated site escape scores of antibodies for epitope group A-F, respectively.  
1019 Epitope groups are distinguished by distinct colors, and the shades show normalized  
1020 site escape scores. Escape hotspots of each epitope group are annotated by arrows.

1021

1022

1023

1024

1025

1026

1027

1028

1029

1030

1031

1032

1033

1034

1035

1036

1037

1038

1039

1040

1041

1042

1043

1044

1045

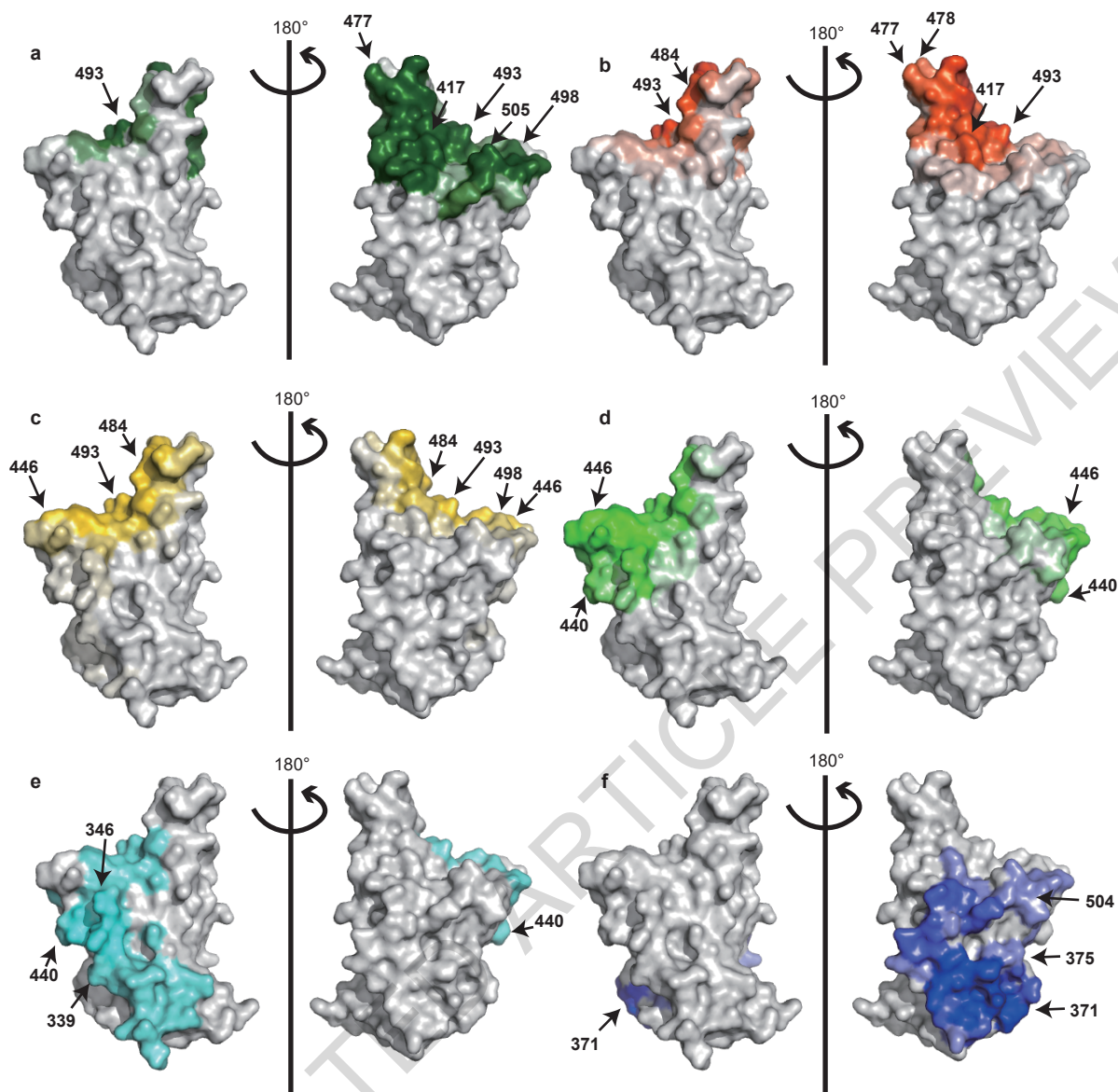
1046

1047

1048

1049

Extended Data Fig. 7



1050 **Extended Data Fig. 7: Antibody-RBD interface distribution for NAbs of each**  
1051 **epitope group.**

1052 **a-f**, Aggregated antibody-antigen interface of antibodies for epitope group A-F,  
1053 respectively. Antibody-antigen interface was indicated from publicly available  
1054 structures of neutralizing antibodies in complex with SARS-CoV-2 RBD. Different  
1055 colors distinguish epitope groups, and the shade reflects group-specific site popularity  
1056 to appear on the complex interface. Shared interface residues (Omicron) of each group  
1057 are annotated.

1058

1059

1060

1061

1062

1063

1064

1065

1066

1067

1068

1069

1070

1071

1072

1073

1074

1075

1076

1077

1078

1079

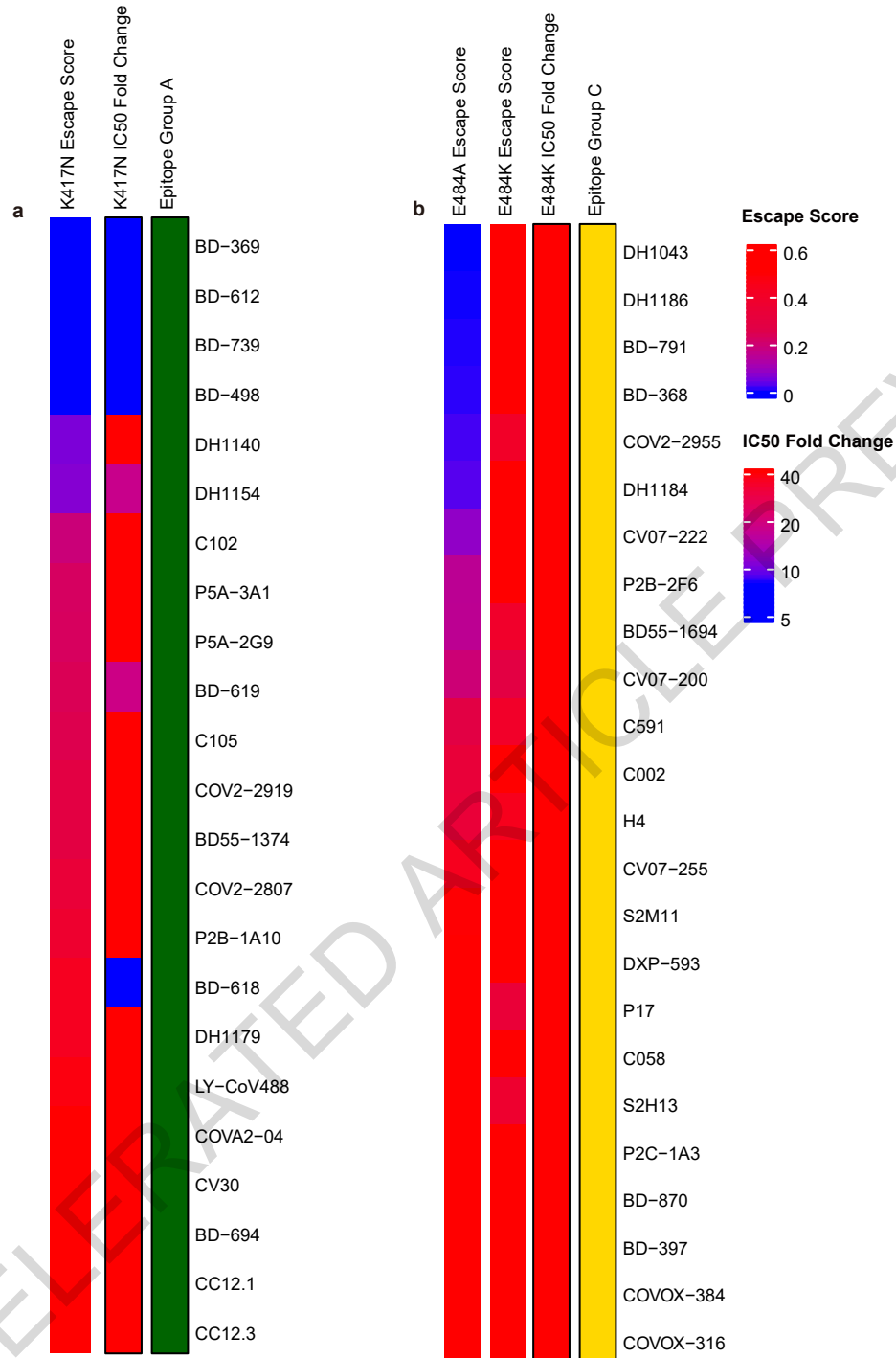
1080

1081

1082

1083

**Extended Data Fig. 8**



1084 **Extended Data Fig. 8: Comparison between mutation escape scores estimated**  
1085 **from yeast display and neutralization of variants carrying corresponding**  
1086 **mutations.**

1087 **a,** K417N escape scores and corresponding K417N pseudovirus neutralizing IC50 fold  
1088 change compared to D614G pseudovirus of antibodies within epitope group A. **b,**  
1089 E484K/E484A escape scores and corresponding E484K pseudovirus neutralizing IC50  
1090 fold change compared to D614G pseudovirus of antibodies within epitope group C.

1091

1092

1093

1094

1095

1096

1097

1098

1099

1100

1101

1102

1103

1104

1105

1106

1107

1108

1109

1110

1111

1112

1113

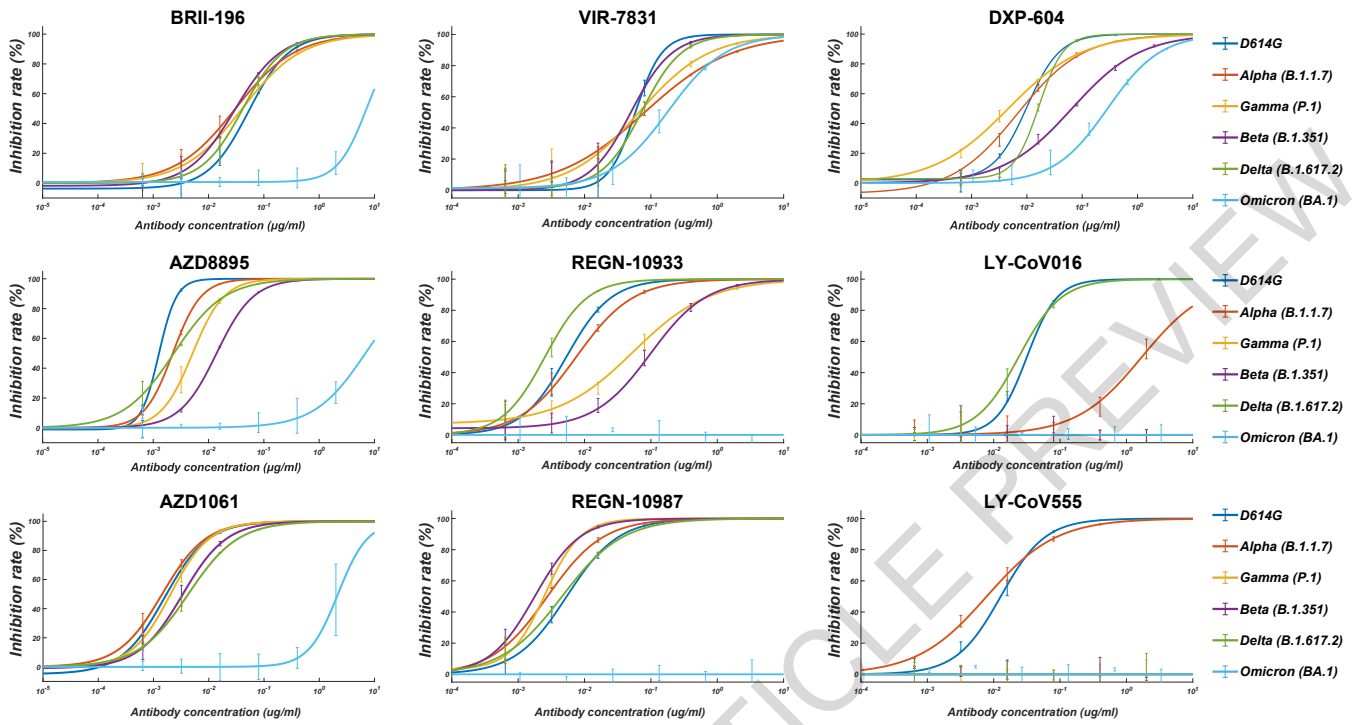
1114

1115

1116

1117

# Extended Data Fig. 9



ACCELERATED ARTICLE

1118 **Extended Data Fig. 9: Pseudovirus neutralization of NAb drugs against SARS-**  
1119 **CoV-2 variants of concern.**

1120 Pseudovirus (VSV-based) assays were performed using Huh-7 cells. Data are collected  
1121 from three biological replicates and represented as mean±s.d.

1122

1123

1124

1125

1126

1127

1128

1129

1130

1131

1132

1133

1134

1135

1136

1137

1138

1139

1140

1141

1142

1143

1144

1145

1146

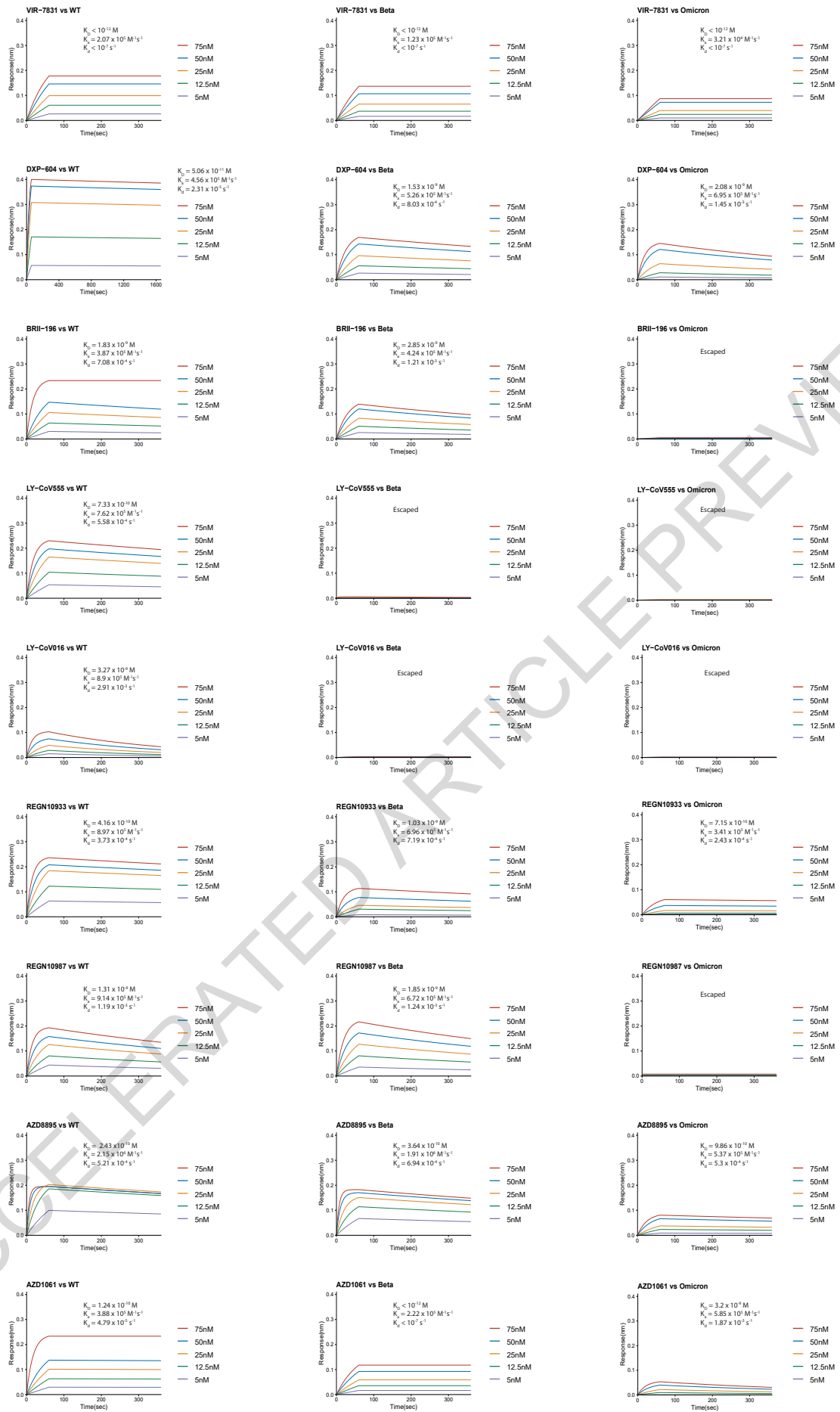
1147

1148

1149

1150

1151



Extended Data Fig. 10

1152 **Extended Data Fig. 10: BLI response between NAb drugs and the RBD of SARS-**  
1153 **CoV-2 wildtype, Beta, or Omicron strain.**

1154 Antibodies were captured by Protein A sensor. The concentrations of RBD are shown  
1155 in different colors. Dissociation constant ( $K_D$ ), association constant ( $k_a$ ), and  
1156 dissociation rate constant ( $k_d$ ) are labeled. NAbs without binding are marked as  
1157 “Escaped”.

1158

1159

ACCELERATED ARTICLE PREVIEW

## Reporting Summary

Nature Portfolio wishes to improve the reproducibility of the work that we publish. This form provides structure for consistency and transparency in reporting. For further information on Nature Portfolio policies, see our [Editorial Policies](#) and the [Editorial Policy Checklist](#).

### Statistics

For all statistical analyses, confirm that the following items are present in the figure legend, table legend, main text, or Methods section.

n/a Confirmed

- The exact sample size ( $n$ ) for each experimental group/condition, given as a discrete number and unit of measurement
- A statement on whether measurements were taken from distinct samples or whether the same sample was measured repeatedly
- The statistical test(s) used AND whether they are one- or two-sided  
*Only common tests should be described solely by name; describe more complex techniques in the Methods section.*
- A description of all covariates tested
- A description of any assumptions or corrections, such as tests of normality and adjustment for multiple comparisons
- A full description of the statistical parameters including central tendency (e.g. means) or other basic estimates (e.g. regression coefficient) AND variation (e.g. standard deviation) or associated estimates of uncertainty (e.g. confidence intervals)
- For null hypothesis testing, the test statistic (e.g.  $F$ ,  $t$ ,  $r$ ) with confidence intervals, effect sizes, degrees of freedom and  $P$  value noted  
*Give  $P$  values as exact values whenever suitable.*
- For Bayesian analysis, information on the choice of priors and Markov chain Monte Carlo settings
- For hierarchical and complex designs, identification of the appropriate level for tests and full reporting of outcomes
- Estimates of effect sizes (e.g. Cohen's  $d$ , Pearson's  $r$ ), indicating how they were calculated

*Our web collection on [statistics for biologists](#) contains articles on many of the points above.*

### Software and code

Policy information about [availability of computer code](#)

Data collection

BLI binding data collections were done by using Octet BLI Discovery 12.2.  
FACS cell sorting were done by using Summit 6.0 (Beckman Coulter).

Data analysis

Neutralization assays were analyzed using PRISM (versions 9.0.1) as described in Methods.  
BLI binding data analyses were done by using Octet BLI Analysis 12.2.  
FACS data were analyzed by FlowJo 10.8.  
V(D)J sequence data were analyzed using Cell Ranger (v6.1.1) and IMGT/DomainGapAlign (v4.10.2).  
Illumina barcodes sequencing data from deep mutational scanning experiments were analyzed using custom scripts (<https://github.com/sunneyxielab/SARS-CoV-2-RBD-Abs-HTDMS>) and package `dms_variants` (v0.8.9).  
Logo plots were generated by Python package `logomaker` (version 0.8).  
For unsupervised clustering, we utilized R function `cmdscale` to convert the cleaned escape matrix into an  $N \times 6$  feature matrix by multidimensional scaling (MDS) with the dissimilarity metric, followed by unsupervised k-medoids clustering within this 6-dimensional antibody feature space, using `pam` function of R package `cluster` (version 2.1.1). Two-dimensional t-Distributed Stochastic Neighbor Embedding (tSNE) embeddings were generated with `Rtsne` package (version 0.15) for visualization. 2D t-SNE plots are generated by `ggplot2` (version 3.3.3), and heatmaps are generated by `ComplexHeatmap` package (version 2.6.2).

For manuscripts utilizing custom algorithms or software that are central to the research but not yet described in published literature, software must be made available to editors and reviewers. We strongly encourage code deposition in a community repository (e.g. GitHub). See the Nature Portfolio [guidelines for submitting code & software](#) for further information.

## Data

Policy information about [availability of data](#)

All manuscripts must include a [data availability statement](#). This statement should provide the following information, where applicable:

- Accession codes, unique identifiers, or web links for publicly available datasets
- A description of any restrictions on data availability
- For clinical datasets or third party data, please ensure that the statement adheres to our [policy](#)

Data availability Processed escape maps for NABs are available in Supplementary Data 1 (as figures), or at <https://github.com/sunneyxielab/SARS-CoV-2-RBD-Abs-HTDMS> (as mutation escape score data). Raw Illumina and PacBio sequencing data are available on NCBI Sequence Read Archive BioProject PRJNA787091. We used vdj\_GRCh38\_alts\_ensembl-5.0.0 as the reference of V(D)J alignment, which can be obtained from <https://support.10xgenomics.com/single-cell-vdj/software/downloads/latest>. IMGT/DomainGapAlign is based on the built-in latest IMGT antibody database, and we let the "Species" parameter as "Homo sapiens" while kept the others as default. FACS-based deep mutational scanning datasets could be downloaded from [https://media.githubusercontent.com/media/jbloomlab/SARS2\\_RBD\\_Ab\\_escape\\_maps/main/processed\\_data/escape\\_data.csv](https://media.githubusercontent.com/media/jbloomlab/SARS2_RBD_Ab_escape_maps/main/processed_data/escape_data.csv). Processed data of this study has been added to this repository as well.

## Field-specific reporting

Please select the one below that is the best fit for your research. If you are not sure, read the appropriate sections before making your selection.

- Life sciences  Behavioural & social sciences  Ecological, evolutionary & environmental sciences

For a reference copy of the document with all sections, see [nature.com/documents/nr-reporting-summary-flat.pdf](https://nature.com/documents/nr-reporting-summary-flat.pdf)

## Life sciences study design

All studies must disclose on these points even when the disclosure is negative.

Sample size	A total of 247 neutralizing antibodies were characterized in the manuscript. No sample size calculation was performed. The sample size of this study is sufficient to obtain sufficient antibodies in each epitope group.
Data exclusions	A total of 271 NABs were initially planned for yeast-display, and 23 NABs failed due to technical errors and could not give any meaningful mutation data.
Replication	Experimental assays were performed in biological duplicate or triplicate according to or exceeding standards in the field. Specifically, we perform MACS-based mutation screening using two independently synthesized mutant libraries. We conducted all neutralization and ELISA assays in biological duplicates or triplicates. All replicates for neutralization and binding assays are successful.
Randomization	Randomization was not required since we were applying a uniform set of measurements across the panel of monoclonal antibodies
Blinding	Blinding was not required since we were applying a uniform set of measurements across the panel of monoclonal antibodies

## Reporting for specific materials, systems and methods

We require information from authors about some types of materials, experimental systems and methods used in many studies. Here, indicate whether each material, system or method listed is relevant to your study. If you are not sure if a list item applies to your research, read the appropriate section before selecting a response.

### Materials & experimental systems

n/a	Involved in the study
<input type="checkbox"/>	<input checked="" type="checkbox"/> Antibodies
<input type="checkbox"/>	<input checked="" type="checkbox"/> Eukaryotic cell lines
<input checked="" type="checkbox"/>	<input type="checkbox"/> Palaeontology and archaeology
<input checked="" type="checkbox"/>	<input type="checkbox"/> Animals and other organisms
<input type="checkbox"/>	<input checked="" type="checkbox"/> Human research participants
<input checked="" type="checkbox"/>	<input type="checkbox"/> Clinical data
<input checked="" type="checkbox"/>	<input type="checkbox"/> Dual use research of concern

### Methods

n/a	Involved in the study
<input checked="" type="checkbox"/>	<input type="checkbox"/> ChIP-seq
<input type="checkbox"/>	<input checked="" type="checkbox"/> Flow cytometry
<input checked="" type="checkbox"/>	<input type="checkbox"/> MRI-based neuroimaging

## Antibodies

Antibodies used

ELISA antibody detection: 109-035-003, Peroxidase-AffiniPure Goat Anti-Human IgG (H+L), Jackson  
 Negative control H7N9 human IgG1 antibody: HG1K, Sino Biology Cat #HG1K  
 The enriched B cells were stained with the following anti-human antibodies and antigens: For every 10<sup>6</sup> cells, 3  $\mu$ L FITC anti-CD19 Antibody (Biolegend, 392508), 3  $\mu$ L FITC anti-CD20 Antibody (Biolegend, 302304), 3.5  $\mu$ L Brilliant Violet 421 anti-CD27 Antibody

(Biolegend, 302824), 3  $\mu$ L PE/Cyanine7 anti-IgM(Biolegend, 314532), and fluorophore-labelled Receptor-Binding Domain (RBD) and ovalbumin (Ova) for 30 min on ice. Cells were stained with 5  $\mu$ L 7-AAD (eBioscience, 00-6993-50) for 10 minutes before sorting. All neutralizing antibodies were expressed using HEK293F cell lines with codon-optimized cDNA and human IgG1 constant regions in house. The detailed sequence could be found in Supplementary Table 1 column I and J.

## Validation

In this manuscript, we tested 247 anti-RBD SARS-CoV-2 human neutralizing IgG1 antibodies. All neutralizing antibodies were expressed using HEK293F cell lines with codon-optimized cDNA and human IgG1 constant regions. All neutralizing antibodies' species and specificity to RBD were validated by ELISA using goat anti-human IgG (H+L)/HRP. All antibodies neutralization ability was verified by VSV-based pseudovirus assays. Details and sequences for all SARS-CoV-2 neutralizing antibodies evaluated in this study is included in Supplementary Table 1. Reactivity and specificity of the primary antibodies listed above is based on the information on manufacturer's homepages.

## Eukaryotic cell lines

### Policy information about [cell lines](#)

## Cell line source(s)

HEK293F for antibody production was received from ThermoFisher (R79007)  
 EBY100 (Yeast) was received from ATCC (ATCCMYA-4941);  
 Huh-7 for pseudovirus assays was received from Japanese Collection of Research Bioresources (JCRB 0403);

## Authentication

No authentication was performed beyond manufacturer standards;

## Mycoplasma contamination

Not tested for mycoplasma contamination;

Commonly misidentified lines  
(See [ICLAC](#) register)

No commonly misidentified cell lines were used in the study.

## Human research participants

### Policy information about [studies involving human research participants](#)

## Population characteristics

The detailed information of SARS-CoV-2 convalescents and vaccinees was previously described in Cao et al., Cell Research, 2021, doi:10.1038/s41422-021-00514-9. Briefly, short-term convalescents' blood samples were obtained at day 62 on average after symptoms onset. Long-term convalescents' blood samples were obtained at day 371 on average after symptoms onset. No vaccination was received before blood collection. SARS-CoV-2 vaccinees' blood samples were obtained 2 weeks after complete vaccination of ZF2001 (RBD-subunit vaccine). For vaccinated SARS-CoV-1 convalescents (average age 58, n = 21), all recruited participants were identified for SARS-CoV-1 infection in 2003, and received two-dose vaccination of CoronaVac and a booster dose of ZF2001 with a 180-day-interval. Blood samples of vaccinated SARS-CoV-1 convalescents were obtained 2 weeks after the booster shot. Three Healthy vaccinated donor (average age 25) were also included to serve as negative control for FACS gating.

## Recruitment

Patients were recruited on the basis of prior SARS-CoV-2 infection or SARS-CoV-1 infection or SARS-CoV-2 vaccination. The only exclusion criteria used were HIV or other debilitating diseases.

## Ethics oversight

Relevant experiments regarding SARS-CoV-2 convalescents and vaccinees were approved by the Beijing Youan Hospital Research Ethics Committee (Ethics committee archiving No. LL-2020-010-K). Relevant experiments regarding SARS-CoV-1 convalescents were approved by the Beijing Ditan Hospital Capital Medical University (Ethics committee archiving No. LL-2021-024-02). Written informed consent was obtained from each participant in accordance with the Declaration of Helsinki. All participants provided written informed consent for the collection of information, and that their clinical samples were stored and used for research. Data generated from the research were agreed to be published.

Note that full information on the approval of the study protocol must also be provided in the manuscript.

## Flow Cytometry

### Plots

## Confirm that:

- The axis labels state the marker and fluorochrome used (e.g. CD4-FITC).
- The axis scales are clearly visible. Include numbers along axes only for bottom left plot of group (a 'group' is an analysis of identical markers).
- All plots are contour plots with outliers or pseudocolor plots.
- A numerical value for number of cells or percentage (with statistics) is provided.

## Methodology

Sample preparation	Whole blood samples from SARS-CoV-2 convalescents or vaccinees were mixed and subjected to Ficoll (Cytiva, 17-1440-03) gradient centrifugation after 1:1 dilution in PBS+2% FBS. After centrifugation, plasma was collected from upper layer and cells were harvested at the interface, respectively. PBMCs were further prepared through centrifugation, red blood cells lysis (Invitrogen™ eBioscience™ 1X RBC Lysis Buffer, 00-4333-57) and washing steps. Samples were stored in FBS (Gibco) with 10% DMSO (Sigma) in liquid nitrogen if not used for downstream process immediately. Cryopreserved PBMCs were thawed in DPBS+2% FBS (Stemcell, 07905). On the day of sorting, B cells were enriched using CD19+ B cell isolation kit according to the manufacturer's instructions (STEMCELL, 19054). Biotinylated receptor binding domain (RBD) of SARS (Sino biological, 40634-V27H-B) or SARS-CoV-2 (Sino biological, 40592-V27H-B) were multimerized with fluorescently labeled Streptavidin (SA) for 1 hour at 4°C. RBD was mixed with SA-PE (Biolegend, 405204) and SA-APC (Biolegend, 405207) at a 4:1 molar ratio. For every 10 <sup>6</sup> cells, 6 ng SA was used to stain.
Instrument	Astrios EQ (BeckMan Coulter)
Software	Summit 6.0 (Beckman Coulter) for cell sorting; FlowJo 10.8 for data analysis.
Cell population abundance	Memory B cell purity post-sorting is over 90% as measured by 10x sequencing.
Gating strategy	Single CD19 or CD20+, CD27+, IgM-, Ova-, RBD-PE+, RBD-APC+, live B cells were sorted on an Astrios EQ (BeckMan Coulter) into PBS containing 30% FBS. The detailed FSC/SSC gating scheme is showed in Supplementary Data 2. Gates are drawn to define positive cells on the basis of unvaccinated healthy donor control.

Tick this box to confirm that a figure exemplifying the gating strategy is provided in the Supplementary Information.